

## BEST AVAILABLE COPY

Initially, Applicants note that after examining the portions of the reference referred to by the Examiner (column 3, lines 27-33 and column 4, lines 24-26), Applicants were unable to find a teaching that the powders of Topchiashvili et al. are non-ferromagnetic and not-cubic. Furthermore, in response to the Examiner's taking Official Notice that the powders of Topchiashvili et al. are non-ferromagnetic and not-cubic, Applicants respectfully disagree.

Initially, Official Notice, which by definition is unsupported by documentary evidence, should only be taken by the Examiner where the facts asserted to be well-known, or to be common knowledge in the art, are capable of "instant and unquestionable demonstration as being well-known." MPEP 2144.03. As also pointed out by this section of the Manual, assertions of technical facts in areas of esoteric technology or specific knowledge of the prior art must always be supported by citation to some reference work recognized as standard in the pertinent art; and it is never appropriate to rely solely on common knowledge in the art without evidentiary support in the record, as the principal evidence upon which a rejection was based.

MPEP 2144.03 further states that if Applicant adequately traverses the Examiner's assertion of Official Notice, the Examiner must provide documentary evidence in the next Office Action if the rejection is to be maintained. Based on the following considerations, Applicants respectfully traverse the Examiner's assertion of Official Notice that the Topchiashvili et al. powders are inherently non-ferromagnetic and not cubic.

Applicants have discovered a method of manufacturing an oriented sintered ceramic product of a new structure which disregards the conventional practice of neglecting magnetic anisotropy of non-ferromagnetic materials, by dispersing a non-ferromagnetic powder having a not-cubic crystal structure into a solvent to prepare a slurry and molding the slurry in a magnetic field, while taking the magnetic anisotropy of the non-ferromagnetic material into consideration. (See page 6, lines 6-15 of Applicants' specification.)

Magnetic susceptibility is a number that characterizes the magnetism of a substance when it is subjected to a magnetic field. (See the attached portion of Encarta World English Dictionary, 2005.) The value of  $1 \times 10^{-6}$  emu/cm<sup>3</sup> is a magnetic

susceptibility that has been conventionally thought to not be affected by a magnetic field. The magnetic susceptibility of alumina is about  $-4 \times 10^6$  emu/cm<sup>3</sup> (see Nature, 164, p 101, 1949), and the magnetic susceptibilities of other materials of the present invention are very small, being about  $-10^{-7}$  emu/cm<sup>3</sup>, which can be treated as zero. [A negative magnetic susceptibility shows that a material is diamagnetic. It is traditionally written as emu/cm<sup>3</sup>, although the volume magnetic susceptibility in cgs (centimeter-gram-second) units is dimensionless and does not have a formal unit.] It has been conventionally assumed, by those of ordinary skill in the art, that these materials are not affected by a magnetic field. Therefore, these materials are used as nonmagnetic materials for equipment which requires nonmagnetic characteristics, such as electronic equipment, semiconductor manufacturing equipment, medical equipment, an electron beam exposure device, etc. Those skilled in the art recognize these materials as nonmagnetic, rather than non-ferromagnetic. Therefore, based upon the knowledge of one skilled in the art, one would not expect these materials, with low magnetic susceptibilities, to be affected by a magnetic field.

On the contrary, the magnetic susceptibility of the superconductive ceramics of Topchiashvili et al. is about  $4 \times 10^{-6}$  emu/cm<sup>3</sup>. [This value is calculated by converting the mass magnetic susceptibility of  $5 \times 10^{-7}$  emu/g (see Nishida et al., page 598, right column, line 4, copy attached) to its equivalent in the emu/cm<sup>3</sup> system by using its density of about 7 g/cm<sup>3</sup>.] It is well known that a material having such a large magnetic susceptibility is affected by a magnetic field.

Based on these considerations, Applicants traverse the Examiner's assertion of Official Notice that the Topchiashvili et al. powders are inherently non-ferromagnetic and not cubic. According to MPEP 2144.03, the Examiner must provide documentary evidence in the next Office Action to support this assertion, if the rejection is to be maintained.

Applicants' claimed invention requires the use of a non-ferromagnetic powder. Topchiashvili et al. do not teach a non-ferromagnetic powder. On the contrary, Topchiashvili et al. use a material with a large magnetic susceptibility,  $4 \times 10^{-6}$  emu/cm<sup>3</sup>, as compared to Applicants' non-ferromagnetic powder with a range of magnetic susceptibility of between  $-4 \times 10^{-6}$  to  $-10^{-7}$  emu/cm<sup>3</sup>, which can be treated as zero.

Although the Examiner takes Official Notice that Topchiashvili et al. teach non-ferromagnetic powders, Applicants' have shown that this is not accurate. The powders of Topchiashvili et al. are magnetic, as shown by their large magnetic susceptibility. Additionally, Topchiashvili et al. do not teach Applicants' discovery of making an oriented sintered ceramic product by disregarding conventional practice of neglecting the anisotropy of non-ferromagnetic materials.

Therefore, Topchiashvili et al. do not teach each and every limitation of Applicants' claim 1, which requires "dispersing a non-ferromagnetic powder having a not-cubic system crystal structure into a solvent to prepare a slurry."

Furthermore, the comments set forth above are equally applicable to claims 2, 12 and 13. Since claims 2, 12 and 13 are directly dependent on claim 1, the subject matter of claims 2, 12 and 13 is patentable over Topchiashvili et al. for the same reasons that the subject matter of claim 1 is patentable over this reference.

For these reasons, the invention of claims 1, 2, 12 and 13 is clearly patentable over Topchiashvili et al.

The rejection of claim 13 under 35 U.S.C. §103(a) as being unpatentable over Topchiashvili et al. is respectfully traversed.

The Examiner states that the teaching of sub-micro particles as well as the use of nano-powders suggest particles that are less than 0.69 microns.

However, as discussed above, Topchiashvili et al. do not teach or suggest a method of manufacturing an oriented sintered ceramic product which comprises dispersing a non-ferromagnetic powder having a not-cubic system crystal structure into a solvent to form a slurry. Topchiashvili et al. do not teach or suggest the limitations of independent claim 1, and therefore, for the same reasons do not teach or suggest the limitations of dependent claim 13.

The rejections of claim 3 under 35 U.S.C. §103(a) as being unpatentable over Topchiashvili et al., and further in view of Wei et al. and as being unpatentable over Topchiashvili et al., and further in view of Takagi et al. are respectfully traversed.

The Examiner admits that Topchiashvili et al. do not disclose the ceramics of claim 3, but the Examiner asserts that it is clear from the reference that the method encompasses materials other than the specific ceramics disclosed. The Examiner states

that Wei et al. disclose the importance of alumina ceramics, and that it would have been obvious to alter the Topchiashvili et al. orienting process by using alumina rather than superconductors, for the advantages of the alumina products.

The Examiner also states that Takagi et al. disclose the difficulty and desirability of creating oriented alumina sintered objects, and that it would have been obvious to apply the Topchiashvili et al. process/ solution to the known alumina problem.

However, as discussed above, Topchiashvili et al. do not disclose a non-ferromagnetic powder, as required in Applicants' claims. Further, there is no teaching or suggestion in Topchiashvili et al. to substitute non-ferromagnetic powders in the superconductors taught in the reference. In fact, the passage relied upon by the Examiner to assert that Topchiashvili et al. encompasses other materials, actually states "modifications and structural changes may be made without departing in any way from the spirit of the present invention." (Emphasis added.) However, the Examiner is suggesting that it would be obvious to substitute a non-ferromagnetic material, such as alumina, which has a magnetic susceptibility which can be treated as zero, for a superconductor material, with a large magnetic susceptibility. This substitution would surely depart from the spirit of the Topchiashvili et al. invention.

Topchiashvili et al. teach the use of a magnetic material, which will certainly be affected by a magnetic field. Topchiashvili et al. do not teach the ability to create an oriented sintered product, using a non-ferromagnetic material and applying a magnetic force, and therefore disregarding the conventional practice of neglecting magnetic anisotropy of non-ferromagnetic materials, by dispersing a non-ferromagnetic powder having a not-cubic crystal structure into a solvent to prepare a slurry and molding the slurry in a magnetic field, while taking the magnetic anisotropy of the non-ferromagnetic material into consideration. Furthermore, neither Wei et al. nor Takagi et al. remedy the deficiencies of Topchiashvili et al.

For these reasons, the invention of claim 3 is clearly patentable over Topchiashvili et al. in view of Wei et al and Topchiashvili et al. in view of Takagi et al.

The rejection of claims 1-3, 12 and 13 under 35 U.S.C. §103(a) as being unpatentable over Morita et al. is respectfully traversed.

The Examiner asserts that Morita et al. disclose the use of colloidal alumina and magnetic fields to form oriented ceramics, but that there is no indication of the strength of the magnetic field. The Examiner states that it would have been obvious to perform routine experimentation to determine what strength of magnetic field would produce the optimal results.

Morita et al. teach that the C-faces of thin tabular or leaf-like tubular ceramics powder are oriented by applying centrifugal force. (See column 2, lines 28-39 of the reference.) In Example 3 of the reference, a centrifugal force and an external magnetic field were applied onto the mixture of strontium ferrite powder and a binder. However, the strontium ferrite is ferromagnetic, and therefore distinct from the non-ferromagnetic powder of Applicants' invention. Furthermore, the reference teaches to apply the magnetic field only in order to further enhance the orientation of M type hexagonal system ferrite, such as strontium ferrite (hexagonal tabular fine grain).

Morita et al. do not teach or suggest a method of manufacturing an oriented sintered ceramic product by dispersing a non-ferromagnetic powder having a not-cubic system crystal structure into a solvent to prepare a slurry, solidifying the mold in a magnetic field and sintering the slurry. The reference does not teach or suggest that the non-ferromagnetic powder is oriented by applying the magnetic field.

Additionally, the Examiner asserts that if one does not consider Morita et al.'s paraffin to be a solvent then the Examiner gives official notice that it is well known to use binder systems that use solvents such as water, and that it would have been obvious to use any conventional binder system that uses a solvent.

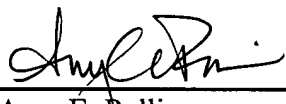
However, when the magnetic field is applied on a ferromagnetic material, such as that in Morita et al., it is not necessary that the particles be suspended, because the magnetic susceptibility of the ferromagnetic material is sufficiently large, and therefore the magnetic field can be applied directly to the particle for orientation of the particle. On the contrary, in the present invention, it is necessary that the particle be suspended in a colloid state for easy rolling since the magnetic susceptibility of the particle is insignificant (can be treated as zero). Therefore, it would not have been obvious to employ a solvent in the teachings of Morita et al., because, the magnetic susceptibility of the material in Morita et al. is large and therefore does not require the use of a solvent.

Therefore, the invention of claims 1-3, 12 and 13 is clearly patentable over Morita et al.

In view of the above remarks, it is submitted that each of the grounds of rejection set forth by the Examiner has been overcome, and that the application is in condition for allowance. Such allowance is solicited.

Respectfully submitted,

Toru SUZUKI et al.

By:   
Amy E. Pulliam  
Registration No. 55,965  
Agent for Applicants

MRD/AEP/pth  
Washington, D.C. 20006-1021  
Telephone (202) 721-8200  
Facsimile (202) 721-8250  
April 20, 2005

## $\mu^+$ SR Studies of Magnetic Properties of the $\text{YBa}_2\text{Cu}_3\text{O}_x$ System

Nobuhiko NISHIDA, Hideaki MIYATAKE, Daisuke SHIMADA,  
Satoshi OKUMA, Masayasu ISHIKAWA,<sup>†</sup> Toshiro TAKABATAKE,<sup>†</sup>  
Yasuhiro NAKAZAWA,<sup>†</sup> Yoshitaka KUNO,<sup>††,†††</sup> Rolf KEITEL,<sup>††</sup>  
Jess H. BREWER,<sup>†††</sup> Tanya M. RISEMAN,<sup>†††</sup> David L. WILLIAMS,<sup>†††</sup>  
Yasushi WATANABE,<sup>††††,†††††</sup> Toshimitsu YAMAZAKI,<sup>††††,†††††</sup>  
Kusuo NISHIYAMA,<sup>††††</sup> Kanetada NAGAMINE,<sup>††††</sup>  
Eduardo J. ANSALDO<sup>†††††</sup> and Eiko TORIKAI<sup>††††††</sup>

*Department of Physics, Tokyo Institute of Technology,  
Ohokayama, Meguro-ku, Tokyo 152*

<sup>†</sup>*The Institute for Solid State Physics, University of Tokyo,  
Roppongi, Minato-ku, Tokyo 106*

<sup>††</sup>*TRIUMF, Vancouver, British Columbia, Canada V6T 2A3*

<sup>†††</sup>*Department of Physics, University of British Columbia, Vancouver, Canada*

<sup>††††</sup>*Meson Science Laboratory, University of Tokyo, Bunkyo-ku, Tokyo 113*

<sup>†††††</sup>*Institute for Nuclear Study, University of Tokyo, Tanashi, Tokyo 188*

<sup>††††††</sup>*Department of Physics, University of Saskatchewan, Saskatoon, Canada  
††††††† Ochanomizu University, Bunkyo-ku, Tokyo 112*

(Received September 14, 1987)

Samples of  $\text{YBa}_2\text{Cu}_3\text{O}_x$  in four different phases have been probed by positive muon spin relaxation ( $\mu^+$ SR) method. Each phase was found to show different magnetic behavior. In the famous orthorhombic 90 K superconductor ( $x \sim 6.9$ ), neither magnetic ordering nor magnetic fluctuations were observed. However, in another orthorhombic superconducting phase ( $x \sim 6.4$ ,  $T_c \approx 60$  K) a magnetic fluctuation was observed below 7 K via muon spin-nuclear spin double relaxation. Its magnetic ordering temperature was expected to be below 2.4 K. Similar behavior was observed in an oxygen-rich ( $x \sim 6.5$ ) tetragonal insulating phase, whereas the oxygen-deficient ( $x \sim 6.2$ ) tetragonal insulating phase was found to be magnetically ordered, most likely antiferromagnetic, near room temperature. This is the first observation of a magnetically ordered state in the  $\text{YBa}_2\text{Cu}_3\text{O}_x$  system.

### §1. Introduction

Announcement of the discovery of superconductivity in La-Ba-Cu oxides at 30 K by Bednorz and Müller<sup>1)</sup> has stimulated a search for new superconductors with still higher transition temperatures ( $T_c$ ) among perovskite type materials; already some Y-Ba-Cu oxides have been found<sup>2)</sup> to become superconducting at 90 K. It seems difficult to explain such a high  $T_c$  in terms of electron-phonon interactions. Possible alternative mechanisms<sup>3)</sup> associated with magnetism have been proposed. In the present paper we report on a microscopic study of the magnetism of the  $\text{YBa}_2\text{Cu}_3\text{O}_x$  system using a positive-muon spin relaxation ( $\mu^+$ SR) method. As  $\mu^+$ SR can be performed

without applying any external field to the sample, it has an advantage over NMR or ESR for the study of magnetism in a superconductor. Furthermore, since the magnitude of the observed  $\mu^+$ SR signal is self-calibrated *a priori* by the incident  $\mu^+$  spin polarization, it is especially useful in studies of disordered systems such as high- $T_c$  superconductors, where NMR or ESR often has a missing signal of unknown magnitude. In an earlier  $\mu^+$ SR study, Nishida *et al.*<sup>4)</sup> reported an observation of some sort of magnetic phase transition in a mixed-phase superconducting sample of Y-Ba-Cu oxide. The present investigation was undertaken to clarify the nature of that transition in single-phase  $\text{YBa}_2\text{Cu}_3\text{O}_x$  samples.

In  $\mu^+$ SR measurements, polarized positive

muons are implanted in the sample where they decay, emitting positrons preferentially along their polarization. We accumulate the numbers of positrons,  $N_F(t)$  and  $N_B(t)$ , emitted in the directions parallel and antiparallel to the incident muon spin at times  $t$  after the muons are implanted into the target. In the sample material muons may experience a magnetic perturbation and lose their initial polarization. This spin relaxation process is described in terms of a longitudinal relaxation function  $G_z(t)$ , which is related to the spatial asymmetry of emitted positrons,  $A(t) = [N_F(t) - N_B(t)] / [N_F(t) + N_B(t)]$ . Through  $A(t)$  we are able to detect local magnetic fields (even if randomly distributed) in a magnetically ordered phase. The method works equally well in zero external field (ZF- $\mu^+$ SR), longitudinal field (parallel to the initial muon polarization, LF- $\mu^+$ SR) and transverse field (TF- $\mu^+$ SR). Details of these methods are described in several review papers.<sup>9)</sup>

The  $\text{YBa}_2\text{Cu}_3\text{O}_x$  system is known to have several different phases, depending upon the oxygen content  $x$ , with physical properties ranging from insulators to superconductors. Recently four distinct metamorphic phases of  $\text{YBa}_2\text{Cu}_3\text{O}_x$  have been synthesized in single-phase states and characterized by Nakazawa *et al.*<sup>6,7)</sup> In the present  $\mu^+$ SR experiment the magnetic properties of these four phases were found to differ drastically. In particular, an insulating sample of the most oxygen-deficient tetragonal phase,  $\text{YBa}_2\text{Cu}_3\text{O}_{6.2}$  was found to order antiferromagnetically near room temperature.

## §2. Samples and Experimental Method

Five samples of four different phases were prepared by appropriate heat treatments in different oxygen atmospheres.<sup>6,7)</sup> Two phases are orthorhombic superconductors and the other two are tetragonal insulators. They are called "Ortho-I" ( $x \sim 6.9$ ), "Ortho-II" ( $x \sim 6.4$ ), "Tetra-I" ( $x \sim 6.5$ ) and "Tetra-II" ( $x \sim 6.2$ ). The oxygen content is known within about 0.1 by neutron scattering experiments on Ortho-I,<sup>10,11</sup> Ortho-II<sup>12)</sup> and Tetra-II.<sup>13)</sup> The oxygen content in Tetra-I was determined by chemical analysis. They are single-phased except for Tetra-I. Ortho-I is the well-known 90

K superconductor. Its lattice parameters are  $a = 3.825 \text{ \AA}$ ,  $b = 3.893 \text{ \AA}$  and  $c = 11.676 \text{ \AA}$ . Its magnetic susceptibility is almost temperature independent in the normal state, with a magnitude of  $5 \times 10^{-7} \text{ emu/gram}$ .<sup>8)</sup> Thus, Ortho-I is a Pauli paramagnet. Ortho-II, more oxygen-deficient than Ortho-I, is also a superconductor with  $T_c \sim 60 \text{ K}$ . Its lattice parameters are  $a = 3.835 \text{ \AA}$ ,  $b = 3.880 \text{ \AA}$  and  $c = 11.744 \text{ \AA}$ . Its magnetic susceptibility in the normal state is slightly smaller than that of Ortho-I and its temperature dependence is weakly Curie-Weiss-like. In Tetra-II, still more oxygen has been removed. Two Tetra-II samples were prepared; one was baked in air at  $907^\circ\text{C}$  and then rapidly quenched to  $77 \text{ K}$  by dropping into liquid nitrogen; the other was similarly quenched from  $770^\circ\text{C}$ . The former sample is considered to contain less oxygen than the latter. Its lattice parameters are  $a = 3.864 \text{ \AA}$  and  $c = 11.803 \text{ \AA}$  for the  $907^\circ\text{C}$ -quenched sample and  $a = 3.865 \text{ \AA}$  and  $c = 11.765 \text{ \AA}$  for the  $770^\circ\text{C}$ -quenched sample. None of the tetragonal samples is superconducting; their electrical resistance shows a semiconductor-like temperature dependence. The magnetic susceptibility<sup>9)</sup> of the Tetra-II samples is smaller than that of Ortho-II at room temperature and shows a slight decrease with decreasing temperature. Toward lower temperatures (below  $20 \text{ K}$ ) it increases Curie-Weiss-like with about  $0.2 \mu_B$  per copper atom. Tetra-I is also an insulator. The lattice parameter  $c$  is smallest among the four phases. Its lattice parameters are  $a = 3.87 \text{ \AA}$  and  $c = 11.63 \text{ \AA}$ . Its magnetic susceptibility obeys a Curie-Weiss law with  $1.1 \mu_B$  per copper atom, but a slight decrease is seen around  $90 \text{ K}$ , presumably due to a trace of superconducting materials in this sample.

Neutron diffraction experiments<sup>10-13)</sup> show which oxygen atoms are removed from the  $\text{YBa}_2\text{Cu}_3\text{O}_x$  crystal as we decrease the oxygen content  $x$ . In these four phases the oxygens in the two-dimensional Cu-O planes that sandwich yttrium atoms remain unchanged. Thus the oxygens that form Cu-O one-dimensional chains<sup>10,11)</sup> between two Ba-O layers of Ortho-I are removed in Ortho-II and Tetra-II. In the present sample of Ortho-II, it was found by neutron diffraction measurements<sup>12)</sup> that two

thirds of the oxygens are missing from the Cu-O chains. Thus, the oxygen content is  $x \sim 6.4$  in the present Ortho-II sample. When more oxygen is removed, a tetragonal phase sets in. In an idealized version of Tetra-II, all the oxygen would be missing from these Cu-O chains.<sup>13)</sup>

The samples for this experiment were sintered polycrystalline discs 30 mm in diameter and 2 mm thick. The  $\mu^+$  SR measurements were performed by using surface muon beam at the M9 meson channel of TRIUMF in Vancouver, Canada and by using pulsed surface muon beam at the  $\pi 1$  channel of the Booster Meson Facility, Meson Science Laboratory, University of Tokyo, Located at KEK. The latter facility was used to see  $\mu^+$  spin relaxation phenomena in a time range longer than  $8 \mu\text{s}$ . The magnetic field at the sample position was kept below 0.2 G for ZF- $\mu^+$ SR measurements.

### §3. Experimental Results

The ZF- $\mu^+$ SR method was applied to Ortho-I, Ortho-II, Tetra-I and Tetra-II samples. Typical examples for each phase are shown in Figs. 1(a)–1(c).

In Ortho-I, which is a 90 K-superconductor, the observed  $G_z(t)$  at 70 K is well represented by a Gaussian Kubo-Toyabe function<sup>14,15,5)</sup>  $G_{zz}^{\text{KT}}(t)$  with  $\Delta \approx 0.12 \mu\text{s}^{-1}$  and  $\tau_c \geq 5 \mu\text{s}$ , as shown in Fig. 1(a). This means that implanted

positive muons are randomly distributed in the crystal and feel no local magnetic field except for the almost static nuclear dipolar fields originating from copper and yttrium nuclei. At 240 K and 315 K motional narrowing of the nuclear dipolar fields was observed. This may be attributed to the onset of  $\mu^+$  diffusion above 200 K. The relaxation function did not show any change at the superconducting transition temperature and retained the same form from 120 K down to 5 K. The  $T_1$  of surrounding nuclei can also be probed by ZF- $\mu^+$ SR. In the present case, the nuclear dipolar field is found to be static, which indicates that the  $T_1$  (or  $T_2$ ) of Cu nuclei in Ortho-I should be longer than  $10 \mu\text{s}$ . We conclude that in Ortho-I there is neither detectable magnetic ordering nor magnetic fluctuations as far as  $\mu^+$  can probe it.

In Ortho-II, which is a 60 K-superconductor,  $G_z(t)$  showed a slow Gaussian damping similar to that observed in Ortho-I, above 80 K. Though there is no drastic change in the spectrum around the superconducting critical temperature,  $G_z(t)$  changes its form gradually with decreasing  $T$ ; the Gaussian damping part is somewhat weakened, as in the case of motional narrowing. Apparently, the nuclear dipolar field fluctuates dynamically. We speculate that this effect may be caused by rapid fluctuation of the surrounding copper

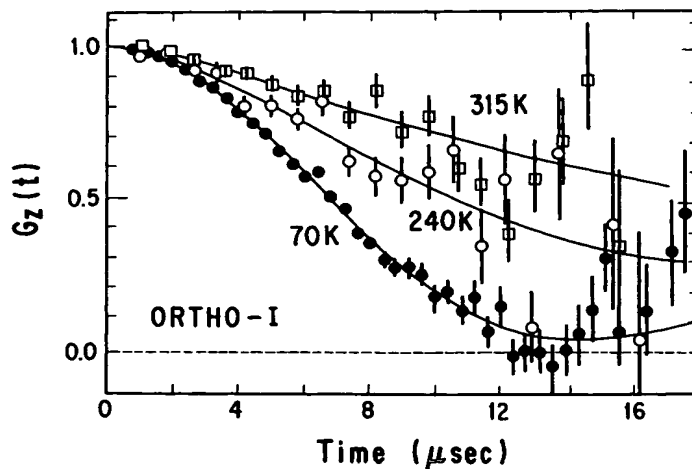


Fig. 1(a). The zero-field  $\mu^+$  spin relaxation functions in Ortho-I (90 K superconductor); the relaxation functions took the same form of a static Kubo-Toyabe function at temperatures from 120 K down to 5 K and the motional narrowing effect, maybe due to  $\mu^+$  diffusion, is seen at 240 K and 315 K.

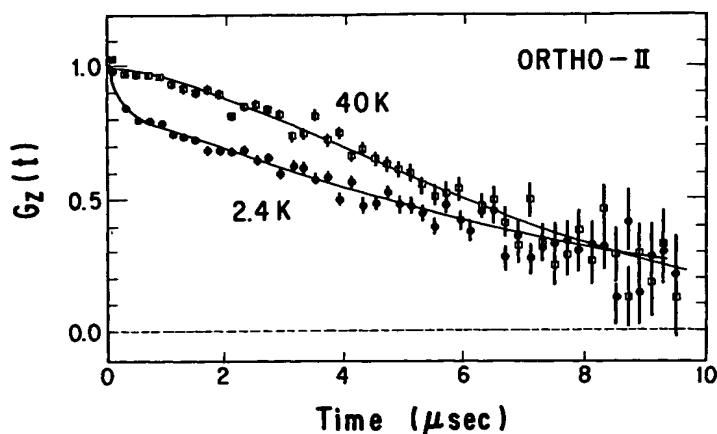


Fig. 1(b). The zero-field  $\mu^+$  spin relaxation functions in Ortho-II (60 K-superconductor); at 40 K, the relaxation function is a Gaussian-type slightly weakened by muon spin-nuclear spin double relaxation mechanism, whereas at 2.4 K the relaxation function changes its form with a fast relaxing part in the time region  $t \leq 300$  ns.

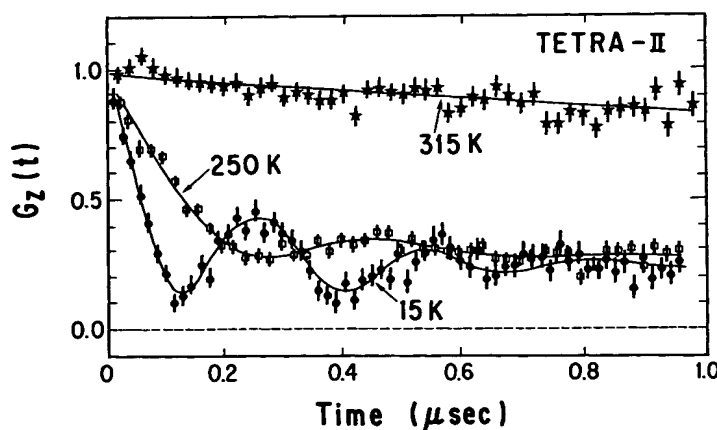


Fig. 1(c). The zero-field  $\mu^+$  spin relaxation functions in Tetra-II (tetragonal insulator); at 250 K and 15 K, the  $\mu^+$  spin precession is shown, with a fast relaxing part in the time region  $t \leq 50$  ns. At 315 K, no precession is observed and Tetra-II is paramagnetic.

nuclei (with a nuclear  $T_1 < 20 \mu\text{s}$ ) due to slowing down of magnetic fluctuation of electrons. When muons are surrounded by magnetic ions, so-called muon-nuclear-spin double relaxation<sup>16)</sup> (first observed in the case of MnSi) may take place; near the magnetic transition temperature the nuclear  $T_1$  in magnetic ions gets shorter than the muon  $T_1$ , and we expect to observe first the narrowing effect of nuclear spin fluctuation on  $G_z(t)$ . Sure enough, this double-relaxation precursor signature is followed at lower temperatures below 7 K by the appearance of a fast-relaxing

component in the early part ( $t < 300$  ns) of  $G_z(t)$ , as shown in Fig. 1(b). This fast relaxing component increased with decreasing temperature. Thus, below 7 K the  $\mu^+$  spin relaxation due to magnetic electrons becomes dominant and Ortho-II may be approaching a magnetic transition, though no definite magnetic ordering was observed down to 2.4 K. Below 7 K, the observed fast relaxing part of  $G_z(t)$  was able to be fitted by a root-exponential function; which suggests as seen in spin glasses<sup>17)</sup> that the magnetism in Ortho-II is disordered one below 7 K and the correla-

tion time of magnetic fluctuations is distributed in a wide time region. This is consistent with recent measurements of the specific heat which has shown a gradual increase, but no peak at low temperatures down to 0.4 K.<sup>8)</sup>

In Tetra-II, an insulator, which is most oxygen deficient, a  $\mu^+$  spin precession signal was observed in zero external field even up to 250 K, for the sample quenched from 907°C, as shown in Fig. 1(c). These precession signals were fitted to a function  $A \exp(-\lambda \cdot t) \cos(2\pi \cdot f \cdot t)$  by a least  $\chi^2$ -method. The fitted precession frequency,  $f$ , is 3–4 MHz and the relaxation rate,  $\lambda$ , is from 3 to  $4 \mu\text{s}^{-1}$  at low temperatures. The observation of  $\mu^+$  spin precession indicates clearly that Tetra-II is in a magnetically long-range-ordered state. It is likely to be antiferromagnetic as the macroscopic magnetic susceptibility is small. This gives the first evidence for magnetic ordering, most likely an antiferromagnetic phase, in the  $\text{YBa}_2\text{Cu}_3\text{O}_x$  system. This precession frequency corresponds to a  $\mu^+$  local field of 250–300 Gauss. The initial amplitude of the precession signal yields the fraction of muons experiencing this local field; this fraction is about 70%\* at low temperatures below 100 K, after the contribution from muons stopped in the sample holder or cryostat walls has been corrected, and gradually decreases with increasing temperature (see Fig. 2(b)).

The observed precession frequency, which is  $\mu^+$  local magnetic field in Tetra-II, increases monotonically toward low temperatures as seen in Fig. 2(a). Below 40 K the temperature dependence shows a peculiar increase. The increase of  $\mu^+$  local magnetic field below 40 K may be explained as follows: At low tempera-

tures the implanted  $\mu^+$  may be trapped at several metastable sites that are not occupied at high temperatures in the oxide and may experience local magnetic fields of a different magnitude there. In fact, this is the case for  $\mu^+$  in  $\text{YFeO}_3$  at low temperatures.<sup>18)</sup> If this occurs in the Tetra-II of  $\text{YBa}_2\text{Cu}_3\text{O}_x$ , the analysis using a single precession frequency might bring about this strange temperature dependence at low temperatures. This problem is still open to question. Above 250 K the precession is hardly recognizable. This may be partially due to the onset of muon diffusion above 200 K, as suggested in Ortho-I, or to a wide distribution of magnetic ordering temperature  $T_N$  as discussed below. Very recently, similar ordering has been observed in another superconductor-related perovskite insulator  $\text{La}_2\text{CuO}_{4-\delta}$  by Uemura *et al.*<sup>19)</sup>

We also observed a fast-relaxing component in Tetra-II, ( $t \leq 50$  ns), as shown in Fig. 1(c). In order to determine whether this fast component (which accounts for about 30%\* of the  $\mu^+$  SR amplitude at low temperatures) is due to inhomogeneous static local fields or to a dynamic magnetic fluctuation, we applied a longitudinal magnetic field parallel to the initial spin direction of the implanted  $\mu^+$ . The fast-relaxing component was found to be decoupled by about 2 kG; we can therefore conclude that it is due to a broad distribution of static local fields, the average field being around 200 G. The amplitude of this component decreased with raising temperature in a similar way to that of the previously mentioned precessing component. As the fast-relaxing component has the same temperature dependence as the precessing component, the origin of random static magnetic fields that bring about the fast relaxation of  $\mu^+$  spins will be the same as that of the local magnetic fields that make a precession of  $\mu^+$  spins. Thus, we consider that the fast-relaxing component may arise from muons occupying defects or disordered sites in the magnetically ordered crystal and experiencing random static fields. Then, from the precessing and fast relaxing components, the magnetically ordered part is nearly 100% of the sample at low temperatures below 100 K.

If the muons feel only these large static local

\* The fraction of muons stopped in materials other than the sample material was determined as follows: A similar shape of MnSi crystal was mounted on the same sample holder in place of  $\text{YBa}_2\text{Cu}_3\text{O}_x$  samples and installed in the cryostat. In MnSi near Néel temperature (about 29.5 K),  $\mu^+$  spin relaxes fast due to critical slowing down phenomena.<sup>16)</sup> Therefore, from the precessing component in TF- $\mu^+$  SR experiments on MnSi around 29 K we are able to determine the fraction of muons stopped in materials other than the sample. We discuss a magnitude of the fraction of muons stopped at some location in the sample, after the fraction of muons stopped in the sample holder or cryostat walls has been subtracted.

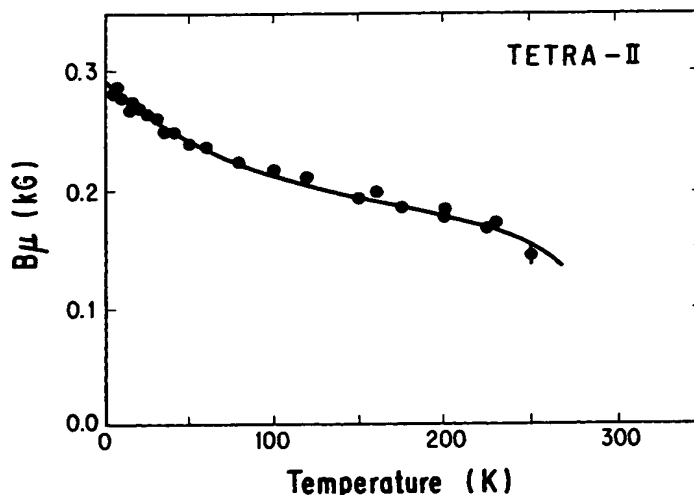


Fig. 2(a). The temperature dependence of internal magnetic fields probed by  $\mu^+$  in the 907°C-quenched sample of Tetra-II.

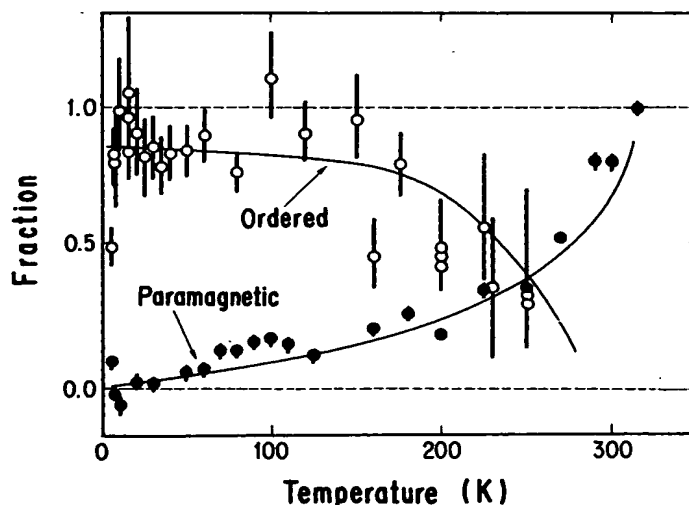


Fig. 2(b). Temperature variation of the relative fractions of the paramagnetic component (• black circles) and the magnetically-ordered component (◦ open circles) in the 907°C sample of Tetra-II.

fields, the ZF relaxation function would asymptotically approach to a value of  $1/3$ . This is actually the case at low temperatures, but at higher temperatures we observe a substantial component whose polarization decays very slowly. The slow relaxation of this component was found to be easily quenched by a small external longitudinal field of 25 G, indicating that the relaxation is due to nuclear dipolar fields as in Ortho-I. Therefore, this component is considered to be paramagnetic

parts in the sample. We applied a small transverse field of 50 G (TF- $\mu^+$ SR) to see a free precession component. After subtracting the contribution\*\* from muons stopped in the materials other than the sample, we found

\*\* The zero-frequency component (c) in the Fourier Transforms includes the contribution from muons stopped in the target holder or cryostat walls as described in the footnote (\*). This is the reason why a peak at zero frequency is seen in the Fourier Transforms at 5 K and 3 K in Fig. 3.

that its fraction is almost zero at lower temperatures and increases with raising temperature. To say in other words, paramagnetic parts in the sample gradually increase with increasing temperature and this tendency becomes striking above 200 K. Finally, at 315 K, all the sample is paramagnetic, as shown in Figs. 1(c) and 2(b). Since the mixture of other phases in the present samples is known to be less than 5% from X-ray diffraction measurements, the increase of the non-magnetic component above 200 K observed here, together with the gradual decrease of amplitude of the 3–4 MHz precession component (see Fig. 2(b)), may be interpreted in terms of a gradual magnetic phase transition (a wide distribution of Néel temperatures in the range 200–300 K). This explains why measurements of static magnetic susceptibility have so far failed to find any magnetic phase transition.<sup>9)</sup>

The longitudinal-field decoupling experiments show that all the local fields reflected in the ZF-relaxation function are static. In this case the local field distribution can be obtained from the Fourier transformation of the relaxation function. These field distributions at various temperatures are demonstrated as Fourier transformations of ZF- $\mu^+$  spin relaxation functions  $G_z(t)$  in Figs. 3(a) and 3(b) for the 907°C-quenched sample and the 770°C-quenched sample, respectively. It consists of (a) discrete fields, which make a broad asymmetric peak around 3–4 MHz and contribute to  $\mu^+$  spin precession, (b) widely distributed fields, whose tail extends beyond a 3–4 MHz peak and brings about the fast relaxing part in  $G_z(t)$ , and (c) nuclear dipolar fields, which correspond to a sharp peak at zero frequency. The components (a) and (b) come from muons occupying sites in magnetically ordered parts of the sample; as discussed before, the former is from muons occupying some interstitial sites and experiencing definite internal magnetic fields and the latter will be from muons occupying disordered sites or defects and feeling random static magnetic fields. The non-magnetic component (c) reflects muons in paramagnetic parts of the sample.

On the Tetra-II sample quenched from 770°C, the similar measurements were per-

formed. The  $\mu^+$  spin precessions of 3.5 MHz, which corresponds to the  $\mu^+$  local field of 270 G, have been observed at temperatures below 10 K, as shown in Fig. 3(b). At 20 K the precession signal was dephased fast and was hardly recognizable as in 907°C-quenched sample above 250 K. And above 100 K the sample was found to be paramagnetic from TF- $\mu^+$ SR. We can say that the 770°C-quenched sample has lower magnetic ordering temperature than the 907°C-quenched sample which contains less oxygen than the former. It is interesting that the observed  $\mu^+$  local field is almost the same below 10 K in these two Tetra-II samples (see Figs. 3(a) and 3(b)), though the magnetic ordering temperature is so different from each other.

We also made ZF- $\mu^+$ SR measurements on Tetra-I. The relaxation functions were nearly the same as those in Ortho-II, although Tetra-I has large magnetic moments of 1.1  $\mu_B$

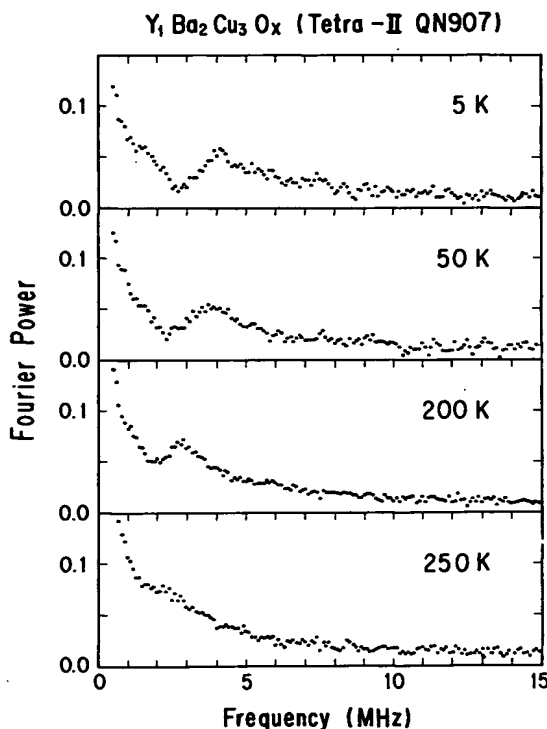


Fig. 3(a). The fourier transformations of the ZF- $\mu^+$  spin relaxation functions,  $G_z(t)$ , for the Tetra-II sample quenched from 907°C (QN907) at various temperatures.

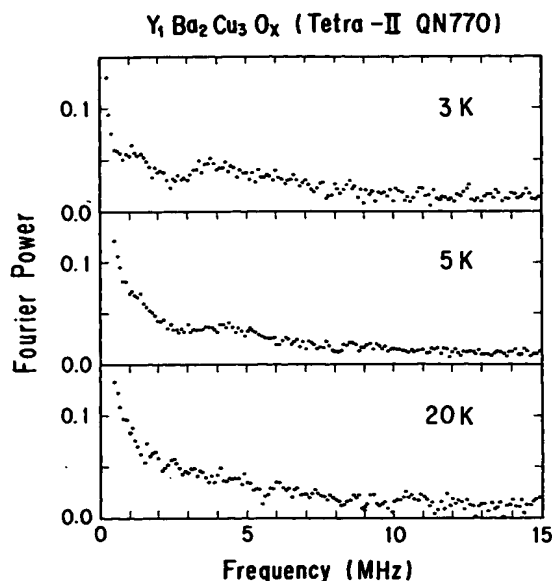


Fig. 3(b). The fourier transformations of ZF- $\mu^+$  spin relaxation functions for the Tetra-II sample quenched from 770°C (QN770) at various temperatures. Please note that the peak near 4 MHz is almost at the same position as that of QN907.

per Cu atom, obeying Curie-Weiss law. There was no magnetic ordering down to 5 K. This makes quite a contrast to Tetra-II.

#### §4. Discussions and Summary

The present  $\mu^+$ SR measurements have clearly shown that the magnetism of the  $\text{YBa}_2\text{Cu}_3\text{O}_x$  system changes drastically with the oxygen content  $x$ . In the following we summarize the experimental results and discuss them briefly.

In Ortho-I ( $x \sim 6.9$ ), a 90 K-superconductor, neither magnetic ordering nor magnetic fluctuations have been observed by  $\mu^+$  at temperatures from 120 K down to 5 K, except for static nuclear dipolar fields of copper and yttrium nuclei. In Ortho-II ( $x \sim 6.4$ ), a 60 K-superconductor; where two thirds of the oxygen atoms are missing in the Cu-O chains of Ortho-I, at high temperatures the magnetic behavior is similar to those in Ortho-I, while with decreasing temperature magnetic fluctuations have been observed and become outstanding below 7 K, although no magnetic ordering has been attained even at 2.4 K. In

Tetra-I ( $x \sim 6.5$ ), an insulator, magnetic properties were found to be similar to those in Ortho-II. In the  $\text{YBa}_2\text{Cu}_3\text{O}_x$  system, oxygen-removal in the Ortho-I seems to cause magnetic moments in the material, though its magnetism is not so strong. We speculate the magnetism in Ortho-II and Tetra-I as follows: By reducing oxygen atoms in Ortho-I, disorder is introduced in the Cu-O chains of Ortho-I, as the neutron scattering experiments<sup>11-13</sup> say that the oxygen occupancy in the two-dimensional Cu-O planes that sandwich yttrium atoms remain unchanged by a change of oxygen content. The disorder might localize electrons around its neighborhood, where the Cu-O chain is cut or disturbed, and bring about magnetism. Thus, magnetism related to this mechanism will be disordered one, as observed by  $\mu^+$ SR experiments of Ortho-II and Tetra-I.

In Tetra-II ( $x \sim 6.2$ ), an insulator where oxygen is most deficient, magnetic properties show a dramatic change. We have observed a  $\mu^+$  spin precession in zero external field even at 250 K for the sample quenched from 907°C. This observation of the  $\mu^+$  spin precession indicates clearly that Tetra-II is magnetically long-range-ordered near room temperature. As the bulk static magnetic susceptibility is small, this magnetic ordering will be antiferromagnetic. From the initial amplitude of  $\mu^+$  spin precession and fast relaxing components, the fraction of magnetically ordered part in the sample was nearly 100% at low temperatures below 100 K. This is the first observation of the presence of an antiferromagnetic phase adjacent to a superconducting one in the  $\text{YBa}_2\text{Cu}_3\text{O}_x$  system. From the TF- $\mu^+$ SR experiment, it was found that the Néel temperature distributes widely from 200 K to 300 K in this sample. In the Tetra-II sample quenched from 770°C, the  $\mu^+$  spin precessions were observed below 20 K and the Néel temperature was found to be below 100 K with a wide distribution. As the 770°C-quenched sample contains more oxygen by a small amount than the 907°C-quenched one, it can be said that the Néel temperature decreases very sharply around the oxygen content between  $x \sim 6.2$  and  $x \sim 6.4$ . However, the  $\mu^+$  local magnetic field observed at low temperatures were about

300 G in these two samples and did not show a large difference. This means that the sub-lattice magnetization does not change so much in spite of a large change of  $T_N$  between these Tetra-II samples. This fact has to be explained by the nature of the antiferromagnetism of Tetra-II. In the previous  $\mu^+$ SR experiment,<sup>4)</sup> we observed a sort of magnetic phase transition around 20 K in a mixed-phase sample of Y-Ba-Cu oxide. It may have relation with this Tetra-II-phase material with the oxygen content near  $x \sim 6.4$ . Of course, other possibilities cannot be rejected.

Here we focus our discussion on the magnetism in Tetra-II. Since yttrium and barium atoms are non-magnetic, the magnetic ordering observed by  $\mu^+$ SR in Tetra-II must be attributed to copper atoms. In the  $\text{YBa}_2\text{Cu}_3\text{O}_x$  system there are two different copper sites; Cu-1 atoms that form one-dimensional Cu-O chains between two Ba-O layers in case of Ortho-I and Cu-2 atoms in the two-dimensional Cu-O planes that sandwich yttrium atoms. If the magnetic ordering were to be ascribed to the electrons of Cu-1 atoms, then the ordering temperature would not be expected to be so high as 250–300 K as observed in 907°C quenched sample, because in Tetra-II the oxygen atoms are absent between neighboring Cu-1 atoms and any super-exchange interaction that brings about such a high Néel temperature as 250–300 K will not be expected between neighbouring Cu-1 atoms. Therefore, magnetic ordering with such a high Néel temperature should be attributed to Cu-2 atoms. In this respect, the magnetic ordering in Tetra-II seems similar to that of  $\text{La}_2\text{CuO}_{4-\delta}$ , where the same two-dimensional Cu-O plane exists and an antiferromagnetic ordering occurs in this plane. To ascribe the magnetism of Tetra-II to Cu-2 atoms is consistent with almost the same sublattice magnetization (the same  $\mu^+$  local fields) in the 907°C and 770°C quenched sample; since the neutron diffraction experiments indicate that the oxygen atoms remain unchanged in two-dimensional Cu-O planes even if the oxygen content is changed, we can expect the same sublattice magnetization at very low temperatures in these two samples after the magnetic ordering has once been established. However, as the

super-exchange interactions between two Cu-2 atoms also will not change, it is difficult to understand the very different  $T_N$ 's in the 907°- and 770°C-quenched samples, where the oxygen content change is by a very small amount and occurs in the neighborhood of Cu-1 atoms. Here, though we do not know the mechanism, we can say that the  $T_N$  is strongly influenced by a change of oxygen occupancy near Cu-1 atoms, that is, a change of the electronic state of Cu-1 atoms. To understand the superconductivity in the  $\text{YBa}_2\text{Cu}_3\text{O}_x$  system, it is the most important question how the oxygen occupancy in the Cu-O chains between two Ba-O layers causes a drastic change of its physical properties from a superconductor (Ortho-I,  $T_c \sim 90$  K, or Ortho-II,  $T_c \sim 60$  K) to an antiferromagnetic insulator (Tetra-II). Therefore, the study of the magnetism of Tetra-II offers important information on the electronic state of  $\text{YBa}_2\text{Cu}_3\text{O}_x$  relevant to an understanding of its superconductivity.

#### Acknowledgements

We would like to thank Professors E. W. Vogt and P. Kitching of TRIUMF for arranging special beam time for the study of high- $T_c$  superconductors. We would like to acknowledge Professor H. Yasuoka for stimulating discussions by informing us of his NMR experimental results on oxide superconductors. We would also like to acknowledge Professors S. Hikami, K. Nagata and H. Kamimura for interesting discussions about high- $T_c$  superconductors. We are grateful to Keith Hoyle and John Worden for the assistance of setting up and maintaining the measuring apparatus, and to Moreno Celi for the data taking. Research at TRIUMF is supported by the Natural Sciences and Engineering Research Council of Canada and, through TRIUMF, by the Canadian National Research Council. The present work is supported by a Grant-in-Aid for Special project Research on Meson Science and a Grant-in-Aid for Overseas Scientific Research of the Ministry of Education, Science and Culture of Japan.

#### References

- 1) J. G. Bednorz and K. A. Müller: *Z. Phys.* B64 (1986) 189.

- 2) S. Hikami, T. Hirai and S. Kagoshima: Jpn. J. Appl. Phys. **26** (1987) L314; C. W. Chu, P. H. Hor, R. L. Meng, L. Gao, Z. J. Huang and Y. Q. Wang: Phys. Rev. Lett. **58** (1987) 2790.
  - 3) P. W. Anderson, G. Baskaran, Z. Zou and J. Hsu: Phys. Rev. Lett. **58** (1987) 2790.
  - 4) N. Nishida, H. Miyatake, D. Shimada, S. Hikami, E. Torikai, K. Nishiyama and K. Nagamine: Jpn. J. Appl. Phys. **26** (1987) L799.
  - 5) Y. J. Uemura and T. Yamazaki: Physica **109-110B** (1982) 1915.
  - 6) Y. Nakazawa, M. Ishikawa, T. Takabatake, H. Takeya, T. Shibuya, K. Terakura and F. Takei: Jpn. J. Appl. Phys. **26** (1987) L682.
  - 7) Y. Nakazawa, M. Ishikawa, T. Takabatake, K. Koga and K. Terakura: Jpn. J. Appl. Phys. **26** (1987) L796.
  - 8) M. Ishikawa, T. Takabatake and Y. Nakazawa: to be published in Physica B (1988).
  - 9) T. Takabatake, M. Ishikawa and T. Sugano: Jpn. J. Appl. Phys. **26** (1987) L1859.
  - 10) F. Izumi, H. Asano, T. Ishigaki, E. Takayama-Muromachi, Y. Uchida, N. Watanabe and T. Nishikawa: Jpn. J. Appl. Phys. **26** (1987) L649.
  - 11) F. Izumi, H. Asano, T. Ishigaki, E. Takayama-Muromachi, Y. Uchida and N. Watanabe: Jpn. J. Appl. Phys. **26** (1987) L1149.
  - 12) M. Ishikawa, T. Takabatake, Y. Nakazawa, H. Asano, T. Ishigaki, F. Izumi and N. Watanabe: in preparation for publication.
  - 13) F. Izumi, H. Asano, T. Ishigaki, E. Takayama-Muromachi, Y. Uchida and N. Watanabe: Jpn. J. Appl. Phys. **26** (1987) L1214.
  - 14) R. Kubo and T. Toyabe: *Magnetic Resonance and Relaxation*, ed. R. Blinc (North-Holland, Amsterdam, 1967) p. 810.
  - 15) R. S. Hayano, Y. J. Uemura, J. Imazato, N. Nishida, T. Yamazaki and R. Kubo: Phys. Rev. **B20** (1979) 850.
  - 16) T. Matsuzaki, K. Nishiyama, K. Nagamine, T. Yamazaki, M. Senba, J. M. Bailey and J. H. Brewer: Phys. Lett. **123A** (1987) 91.
  - 17) Y. J. Uemura, T. Yamazaki, D. R. Harshman, M. Senba and E. J. Ansaldo: Phys. Rev. **B31** (1985) 546.
  - 18) E. Holzschuh, W. Kündig and A. B. Denison: Hyperfine Interactions **17-19** (1984) 345.
  - 19) Y. J. Uemura, W. J. Kossler, X. H. Yu, J. R. Kempton, H. E. Schone, D. Opie, C. E. Stronach, D. C. Johnson, M. S. Alvarez and D. P. Goshorn: Phys. Rev. Lett. **59** (1987) 1045.
-

Print Preview **magnetic susceptibility** [back to Dictionary Results View](#)

On the File menu, click Print to print the information.

**mag·net·ic sus·cep·ti·bil·i·ty**

noun

**number characterizing magnetization of substance:** a number that characterizes the magnetization of a substance when it is subjected to a magnetic field.

*Also called* susceptibility

Encarta® World English Dictionary [North American Edition] © & (P)2005 Microsoft Corporation. All rights reserved.  
Developed for Microsoft by Bloomsbury Publishing Plc.

## Atomic ordering reaction and associated variation of magnetic coercivity of oriented L1<sub>0</sub>-FePt nanoparticles

Kazuhisa Sato\*, Bo Bian<sup>a</sup> and Yoshihiko Hirotsu

The Institute of Scientific and Industrial Research, Osaka University, 8-1 Mihogaoka, Ibaraki, Osaka 5670047, Japan

<sup>a</sup>Presently at: Carnegie Mellon Univ., Pittsburgh, PA 15213-3890, USA

Atomically ordered FePt nanoparticles (L1<sub>0</sub>-type structure) covered with amorphous (a-) Al<sub>2</sub>O<sub>3</sub> have been fabricated. In this process, Fe particles were deposited on Pt "seed" particles which were epitaxially grown on (100) NaCl or MgO substrates. Annealing the a-Al<sub>2</sub>O<sub>3</sub>/FePt films at temperatures higher than 773 K leads to a formation of ordered nanoparticles with mutual fixed orientation in a monolayer form. Three variant ordered domains of the tetragonal L1<sub>0</sub> structure coexisted in a single nm-sized FePt particle, even in a particle as small as 7 nm. According to in-situ electron diffraction study, the degree of order of the ordered structure started to increase on annealing at 773 K and almost saturated on annealing at 873 K for 16 h. The magnetic coercivity varied depending on the particle size and the degree of order in the L1<sub>0</sub> structure formation. The perpendicular coercivity exceeded the in-plane one during the annealing. The in-plane coercivities of FePt nanoparticles measured both parallel to [100]<sub>MgO</sub> and [010]<sub>MgO</sub> directions were almost equal in numerical value. These results reflect the ordered domain formation process and the volume fraction of the domains. Remanent magnetization decay measured for the in-plane magnetization revealed a magnetic relaxation with the type of magnetic dipolar interaction between the FePt particles.

**Key words:** Atomic ordering, L1<sub>0</sub>-FePt, Amorphous Al<sub>2</sub>O<sub>3</sub>, HRTEM, Hard magnetism, High-density recording, Thermal fluctuation, Remanent magnetization decay.

### Introduction

Recently, the magnetic recording density has become higher year by year and reached nearly the maximum value (around 1 Gbit/in<sup>2</sup> [1]) for the conventional recording media with continuous magnetic thin films. It is predicted that the density of magnetic recording will reach to 10 to 100 Gbits/in<sup>2</sup> [2-4] during the years between 2001 and 2006 according to today's rate of progress [4]. The grain sizes of recording media have been decreasing to increase the recording density. As the candidates for near future high-density recording media, films including FePt and CoPt ordered alloy nano particulates, called "nano-granular films" have been attracting much attention in recently [5-7]. These alloy nanoparticles include atomic ordering reactions from disordered fcc phase to ordered L1<sub>0</sub> phase [8] (CuAu I-type structure) in their fabrication processes. The ordered structure of these alloys have a large magnetocrystalline anisotropy energy as high as 10<sup>6</sup> to 10<sup>7</sup> J/m<sup>3</sup> [9-10], which is one hundred times larger than that of bcc-Fe. When the volume of the magnetic particles decreased, the thermal fluctuation of magnetization affect the magnetization of particles, and cause the disappearance of memorized information. Shimatsu

*et al.* discussed the effect of thermal fluctuation of magnetic moment on the ordered L1<sub>0</sub>-FePt nanogranular film [12]. The particle morphology, size, crystallographic orientation and inter-particle distance are strongly dependent on the fabrication process, and these parameters affect their magnetic properties largely. For example, the magnetic coercivity of Fe nanoparticles shows peculiar dependence on the inter-particle distance [13], and the particle size [14]. From the practical viewpoints as the longitudinal magnetic recording media, the easy axis of the material, which is usually related to their crystallographic structure, have to be oriented parallel to the film plane. Also, as the magneto-optical or perpendicular recording media, the easy axis has to be aligned perpendicular to the film plane. However few studies have reported the orientation control in nano-particulate systems, in spite of many approaches for epitaxial growth performed in FePt and CoPt thin continuous films [11, 15-20]. The present authors have reported the structure and magnetic properties of oriented L1<sub>0</sub>-FePt nanoparticles on amorphous (a-) Al<sub>2</sub>O<sub>3</sub> thin film [21-24]. In this paper, we report our recent study of FePt nanoparticles, especially, on their atomic ordering reactions and the related variation of magnetic properties.

### Experimental Procedures

Thin films of oriented FePt nanoparticles covered with

\*Corresponding author.  
Tel : +81-6-6879-8431  
Fax: +81-6-6879-8434  
E-mail: sato@sanken.osaka-u.ac.jp

amorphous  $\text{Al}_2\text{O}_3$  were fabricated using an electron-beam evaporation technique in a high-vacuum chamber with a base pressure of approximately  $3 \times 10^{-7}$  Pa. The process took advantage of the overgrowth of bcc-Fe on fcc-Pt "seed" particles, which were epitaxially grown on (100) NaCl and MgO substrates kept at 673 K during the deposition [21-22], and also of an ordering reaction between Fe and Pt on annealing at temperatures higher than 773 K. A quartz thickness monitor was attached in the chamber to estimate the average thickness of the deposited layers. First, Pt particles were deposited with a rate of 0.1 to 0.5 nm/min on both of the NaCl and MgO substrates set side by side and kept at 673 K. Successively, Fe was deposited onto the substrates at a deposition rate of 0.3 to 1.0 nm/min. In order to protect the deposited Fe from oxidation, a cover layer of  $\alpha\text{-Al}_2\text{O}_3$  with a thickness larger than 4 nm was deposited without breaking vacuum. The averaged thicknesses of the "seed" Pt particle layers were set to be 0.5 to 1.5 nm and that of Fe ranged from 0.5 to 3.5 nm. A part of the NaCl (100) substrate with the as-deposited or after-annealed films was immersed in distilled water and the deposited films removed were mounted onto copper microgrids for later transmission electron microscopy (TEM) observations with 200 and 300 kV electron microscopes. Annealing of the specimens were mainly performed in a vacuum furnace with a pressure less than  $2 \times 10^{-5}$  Pa at 873 K for several hours. Because of the epitaxial relations between the substrate and Pt ( $\langle 011 \rangle_s // \langle 011 \rangle_{\text{Pt}}$ ,  $\{100\}_s // \{100\}_{\text{Pt}}$ ), and between Pt and Fe ( $\langle 100 \rangle_{\text{Fe}} // \langle 100 \rangle_{\text{Pt}}$ ,  $\{011\}_{\text{Fe}} // \{010\}_{\text{Pt}}$ ) [21-22], the  $\text{L}_{10}\text{-FePt}$  nanoparticles observed by TEM were found to be grown mutually under a fixed orientation. The atomic ordering reactions were studied by in-situ TEM observation using a specimen heating stage. The composition analysis of the specimen was done by energy dispersive X-ray spectroscopy

(EDS) apparatus, which was attached to the TEM. Magnetization hysteresis loops of the films on NaCl and MgO substrates were measured with a superconducting quantum interference device (SQUID) magnetometer in the temperature range from 10 to 300 K. No appreciable difference between magnetic data from the films on NaCl and MgO was observed. Thermomagnetic magnetization decay was also measured using SQUID as follows. At first, we applied the field of 10 kOe parallel to the film plane and abruptly removed it to 0, followed by measuring the decay curve for around  $10^3$  min.

## Results and Discussion

### Structural change by atomic ordering

Figure 1 shows three examples of selected area electron diffraction (SAED) patterns taken from an  $\alpha\text{-Al}_2\text{O}_3/\text{Fe}$  (44 at.%) / Pt (56 at.%) film at 300, 773 and 873 K in the course of annealing in TEM. These SAED patterns were received using imaging plates. Each of these patterns was taken after keeping 10 min at each temperature. In the pattern for the as-deposited (300 K) condition, fcc-Pt and bcc-Fe coexists satisfying the epitaxial orientation relationship [21-22] mentioned in the experimental procedures. A halo-pattern from the  $\alpha\text{-Al}_2\text{O}_3$  can be seen as the background. At 773 K, weak superlattice reflections started to be seen, though weak spots from the residual bcc-Fe are still observed. At 873 K, superlattice reflections became strong, and reflections from the residual bcc-Fe disappeared. This result indicates that the alloying process of Pt and Fe, and the atomic ordering process from disordered Fe-Pt to the ordered  $\text{L}_{10}\text{-FePt}$  structure (CuAu I-type) occurred almost simultaneously. The change of SAED intensity profiles with the annealing temperature are shown in Fig. 2, which were measured along  $[001]_{\text{FePt}}$

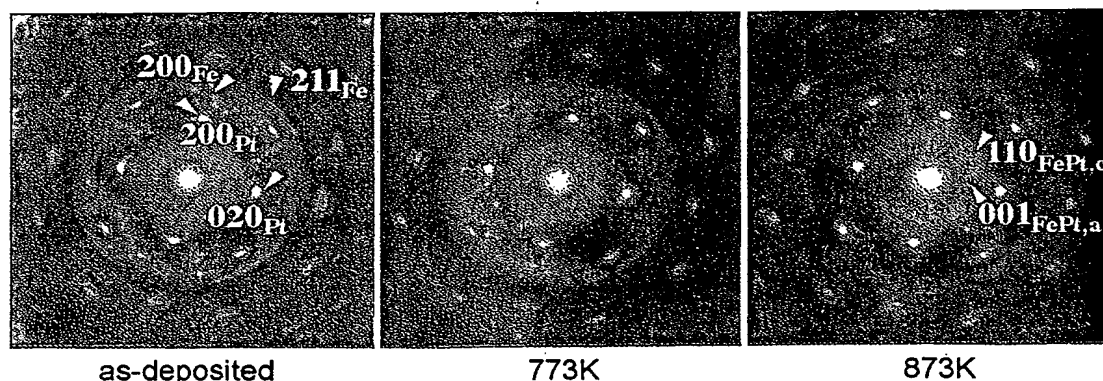


Fig. 1. Three examples of SAED patterns of an  $\alpha\text{-Al}_2\text{O}_3/\text{Fe}$  (44 at.%) / Pt (56 at.%) film at 300, 773 and 873 K extracted from the in-situ observation in the temperature range from 300 to 873 K. The superlattice reflections gradually appeared with increasing the annealing temperature, and on the contrary, the reflections from the residual bcc-Fe disappeared simultaneously. The spotty diffraction patterns mean the existence of mutual orientation relationships between the FePt nanocrystallites (fcc-Pt and bcc-Fe at 300 K). In the pattern for 873 K, the superreflections  $110_{\text{FePt},c}$  and  $001_{\text{FePt},a}$  come from the structural domains with c-axis normal and parallel to the film, respectively.

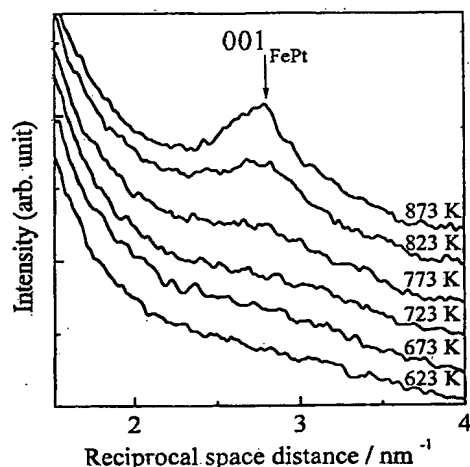


Fig. 2. The SAED intensity profiles for different temperatures measured along the  $[001]_{\text{FePt}}$  direction in the pattern. Superlattice reflection position is shown by the arrow in the figure. Intensity of the ordered reflection  $001_{\text{FePt}}$  appeared at 773 K and gradually enhanced with increasing the annealing temperature.

direction in the pattern. A broad peak of superlattice reflection can be seen above 773 K in Fig. 2. Similarly, a broad peak of superlattice reflection was visible above 773 K in the profiles measured along  $[110]_{\text{FePt}}$  direction.

Figure 3 shows the annealing time dependence of diffracted beam intensity ratio of 110 superlattice reflection to 220 fundamental reflection obtained by in-situ SAED observation performed at 873 K using the same specimen as in Fig. 1 and 2 (Fe-56 at.% Pt). The measurement error represents the standard deviation of measured intensities at each data point. The particles observed by TEM did not coalesce even after the temperature reached at 873 K. At the initial stage of

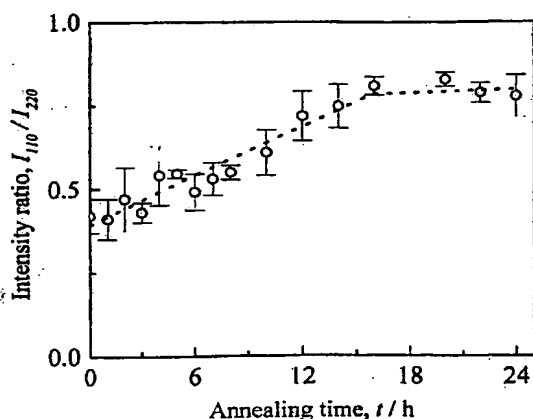


Fig. 3. Variation of intensity ratio of 110 superlattice reflection to 220 fundamental one against the annealing time under 873 K. During the annealing, the specimen thickness could be regarded as constant because of after no particle cohesion on annealing. The increase of 110 reflection intensity was saturated after 16 h annealing.

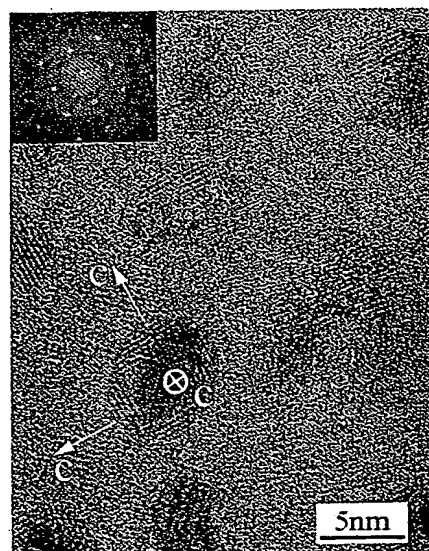


Fig. 4. Lattice fringe images of the FePt nanoparticles and the corresponding SAED pattern for an  $\alpha\text{-Al}_2\text{O}_3/\text{Fe}$  (40 at.%) / Pt (60 at.%) film after annealing at 873 K for 1 h. Ordered FePt particles with mean sizes of 8 nm are homogeneously dispersed. Also the ordered domain structures can be seen in the particles. In each particle, the central region corresponds to the domain with the  $c$ -axis normal to the film plane and the outer regions corresponds to the domains with the  $c$ -axes parallel to the film plane.

annealing, the intensity ratio of 110 to 220 increased linearly, followed by the saturation after about 16 h. Since the dynamical effect in electron diffraction often makes the quantitative interpretation of diffraction intensities difficult. It was difficult to evaluate the accurate long-range order parameters from the SAED patterns. However, since the particles did not change their external shape appreciably during the aging mentioned above, the particle thickness must be almost constant during the annealing. So the saturation of the  $I_{110}/I_{220}$  ratio in Fig. 3 can be regarded as the end of ordering reaction. This data is useful for us to decide the appropriate annealing time for sufficient ordering.

In this study, we fabricated various sizes of FePt nanoparticles with average sizes from 8 nm to 20 nm. Figure 4 shows the FePt nanoparticles fabricated with the mean sizes of 8 nm. We have reported in our previous work that three-variant ordered crystalline domains of the  $L1_0$  phase could coexist even in nano-sized FePt nanoparticles [21-22]. Such ordered variants can also be seen in small particles even as small as 7 nm in the middle of Fig. 5. This result could be explained by the equivalent chance for nucleation and growth of domains with the three variant crystallographic orientations on the substrate. The easy axis of magnetization in the  $L1_0$ -FePt structure is  $c$ -axis, so the existence of these ordered domains would greatly affect the magnetization process and magnetic properties of the particles. The reason why such domains coexist irrespective of energetically unfavorable situation is unknown at this

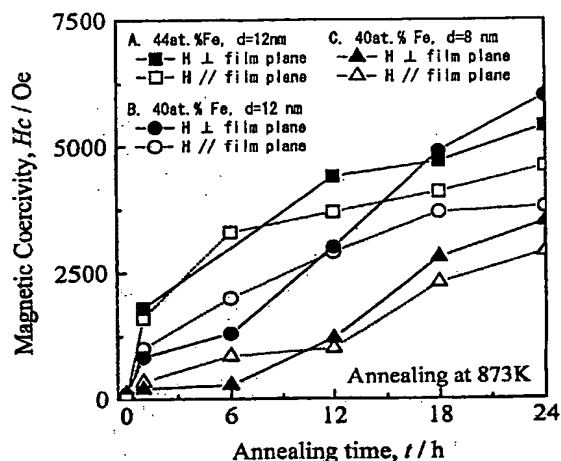


Fig. 5. Variation of magnetic coercivity against the annealing time under 873 K for two kinds of specimen with different mean particle diameters. The coercivities both normal and parallel to the film plane are enhanced with increasing the annealing time, though their coercive forces are reversed after annealing for 10 h.

moment.

#### Variation of magnetic properties due to atomic ordering

Annealing time dependence of coercivities was plotted in Fig. 5. The data marked by square (sample-A) were obtained from the same specimen as observed in Fig. 1 to 3 (mean particle diameter: 12 nm, mean composition: Fe-56 at.% Pt). Another data points marked by circles (sample-B) and triangles (sample-C) were obtained from the specimens with the mean particle sizes of 12 and 8 nm, respectively. Both of them had the averaged concentration of Fe-60 at.% Pt. Coercivities of these specimens showed a similar tendency to the annealing time. At the initial stage of annealing (< 10 h), the in-plane coercivities were larger than the perpendicular one, however, this relationship was reversed when annealed longer than 10 to 12 h. It is considered that the large enhancement of coercivity on annealing is due to the atomic ordering from cubic to tetragonal phase with the higher magnetocrystalline anisotropy. The reversal of the gradient of coercivity change with annealing time must be related to a reversal of volume fractional change of the variant structural domains, the volume of the domain with the c-axis normal to the film plane becomes larger than either of the volume of domain with the c-axis parallel to the film plane. The coercivity change of sample-A on annealing must be closely related to the increase of degree of order of  $L1_0$ -structure as seen in Fig. 3. However, for the perpendicular and in-plane magnetizations in sample-B and -C, the coercivity reversal was clearly observed after 12 h annealing, and after the reversal, the coercivity difference for the smaller particles is smaller compared with that for the larger particles. So it is considered that the alloy concentration and particle size affect the atomic order-

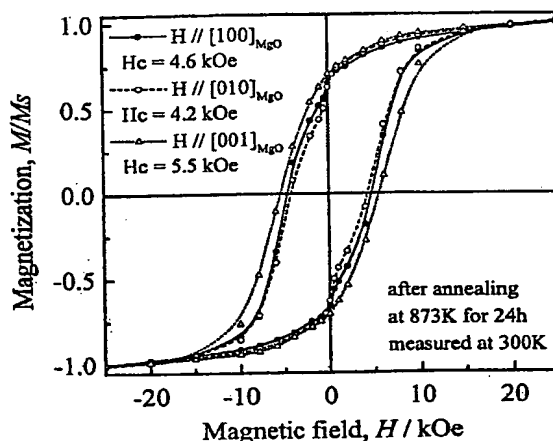


Fig. 6. Typical magnetization vs. magnetic field (M-H) loops for a- $\text{Al}_2\text{O}_3/\text{Fe}$  (44 at.%)/Pt (56 at.%)/MgO(100) films measured at 300 K after annealing at 873 K for 24 h. These three loops were measured using the applied field parallel to the three equivalent principle axes of MgO substrate. The perpendicular coercivity slightly exceeded both of the plane coercivities.

ing process and the ordering domain formation. The smallest averaged particle size with a high coercivity (3.5 kOe) obtained so far was 8 nm after annealing at 873 K for 24 h (see solid triangles in Fig. 5).

Figure 6 shows the applied field direction dependence on the hysteresis loop for the specimen with mean particle diameter of 12 nm and the composition of Fe-56 at.% Pt after annealing at 873 K for 24 h. Under the epitaxial orientation relationship, three variants of  $L1_0$ -domains are epitaxially grown on the MgO-substrate. So we induced the field parallel to the direction of  $[100]_{\text{MgO}}$ ,  $[010]_{\text{MgO}}$ , these are ("in-plane" direction), and also to  $[001]_{\text{MgO}}$  (perpendicular direction). The perpendicular coercivity exceeded the in-plane one and the in-plane coercivities measured both parallel to  $[100]_{\text{MgO}}$  and  $[010]_{\text{MgO}}$  were almost the same. This result can be expected by the existence of three kinds of variant structural domains mentioned above. From the shape and the squareness of M-H loops with three different magnetic field directions shown in Fig. 6, it is found that the easy axis directions of the film are along the three applied magnetic fields.

#### Effect of thermal fluctuation on magnetic properties

We studied the temperature dependence of coercivity, since it is expected that the lower the temperature, the smaller the thermal fluctuation becomes. The ratios of coercivities measured at 300 and 10 K ( $H_c(300\text{ K})/H_c(10\text{ K})$ ) are presented in Fig. 7 for three specimens with different particle sizes (8 to 14 nm), but have the same averaged composition (Fe-60 at.% Pt) and the same packing density around 0.3 to 0.4. All these specimens were annealed at 873 K for 1 h after the deposition, and are supposed to have almost the same ordered structures. In case of the specimen with sufficiently

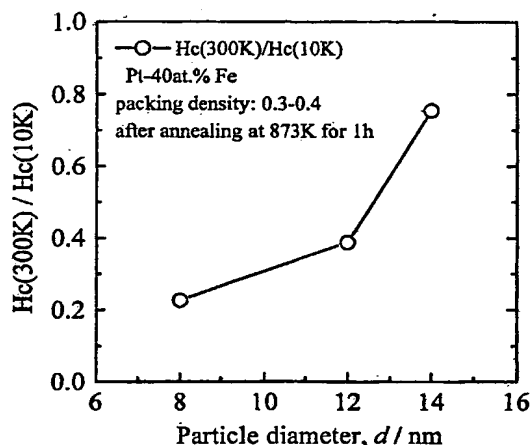


Fig. 7. Mean particle size dependence of coercivity ratio measured at 300 K and 10 K. In case of the specimen with sufficiently large particle diameter, this ratio ought to be near unity. However, in case of nanoparticles with small sizes, this ratio would decrease below unity, depending on the magnitude of thermal fluctuation, which depends on the particle volume.

large particle diameter, the ratio ( $H_c(300\text{ K})/H_c(10\text{ K})$ ) must be near unity, since the thermal agitation would not affect it seriously because of the thermal stability owing to the high magnetocrystalline anisotropy. However, in case of nanoparticles with small sizes, this ratio would decrease far below unity, depending on the magnitude of thermal fluctuation. Especially in the case of annealing time for 1 h, the ratio rapidly decreased with decreasing the particle diameter, and reached 0.2 for the size of 8 nm. These results strongly suggest the size-dependence of thermal fluctuation for the present FePt nanoparticles, especially for the particle size below about 10 nm.

In order to investigate the correlation of magnetic interaction between the particles, the thermoremanent magnetization decay curve was measured at 300 K with the specimen used in the measurement shown in Fig. 6 ( $a\text{-Al}_2\text{O}_3/\text{Fe}(44\text{at.}\%)/\text{Pt}(56\text{at.}\%)/\text{MgO}(100)$ ). In Fig. 8, the residual magnetization decreased with time and saturated after  $10^3$  min. Their total decay value was about 3%. This decay curve showed the peculiar time dependence different from the Néel model [25] for non-interacting isolated particles, which represents the magnetization decay as

$$M_r(t) = M_0 e^{-t/\tau} \quad (1)$$

, where  $M_r(t)$  is the time dependent remanent magnetization,  $M_0$  the initial remanent magnetization,  $t$  the time and  $\tau$  the relaxation time. This expression can be rewritten as  $\log M_r(t) \propto -t$ . However, our result showed the log-log type time dependence, that is,

$$\log M_r(t) \propto -\log t \quad (2)$$

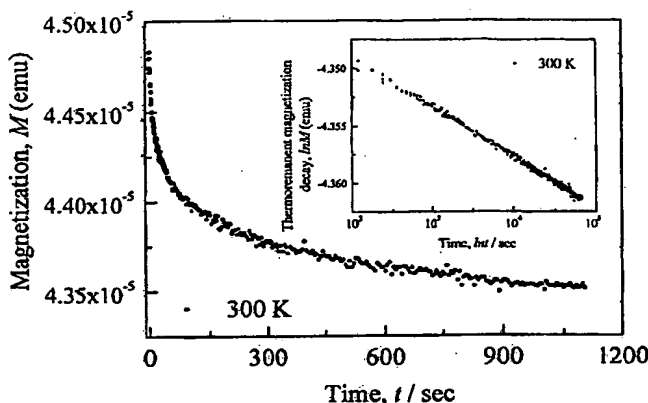


Fig. 8. Remanent magnetization decay curve measured at 300 K with the specimen used in measurement shown in Fig. 7 ( $a\text{-Al}_2\text{O}_3/\text{Fe}(44\text{at.}\%)/\text{Pt}(56\text{at.}\%)/\text{MgO}(100)$ ), after annealing at 873 K for 24 h. The residual magnetization decreased with time and saturated after  $10^3$  min. Their total decay value is about 3%. The curve represented by log-log scale is shown in the inset.

as shown in the inset of Fig. 8. Relaxation relationships different from Néel model were discussed both theoretically [26] and experimentally [27] from the viewpoint of intergranular magnetic interactions. Our recent study indicated the existence of weak intergranular magnetic dipole interaction using the  $\delta M$  plot [24]. The observed slow relaxation can also be attributed to the thermal fluctuation of magnetization even after the atomic ordering under the weak intergranular magnetic dipole interaction [27]. Thermal fluctuation of magnetization is a serious problem for magnetic recording media, because it results in obscurity of the stored memory. From the viewpoint of high coercivity with high anisotropy,  $L1_0$ -FePt has a great possibility against the thermal fluctuation, but as the magnetic recording media, less intergrain interactions are also necessary. Also, it is said that too much coercivity owing to the huge anisotropy results in the poor overwrite performance [12].

## Summary

Annealing of 2-dimensionally dispersed Fe/Pt nanoparticles on MgO and NaCl single crystal substrates at temperatures higher than 773 K leads to a formation of the ordered nanoparticles with mutual fixed orientation. Three variant ordered domains of the tetragonal  $L1_0$  structure coexisted in single nm-sized FePt particle after annealing at 873 K. The magnetic coercivities varied depending on the annealing time at 873 K, the particle size and the measuring temperature. Even for the smallest averaged particle size of 8 nm, a high coercivity of about 3.5 kOe was observed. According to in-situ electron diffraction study, the degree of order of the FePt structure started to increase on annealing at 773 K and saturated on annealing at 873 K for 16 h. The magnetic hardening due to the atomic ordering was shown experimentally in nm-sized FePt particles.

The remanent magnetization decay curve showed a relation  $\log M \propto -\log t$ , and the slow relaxation expressed by this relationship could be explained due to the inter-granular magnetic dipole interaction.

### Acknowledgements

The authors wish to thank Prof. T. Kawai and Dr. H. Tanaka of ISIR, Osaka University for support of the SQUID measurement. This study was supported by the Center of Excellence (COE) program of the Japanese Ministry of Education, Science, Sports and Culture.

### References

1. R.L. White, R.M.H. New and R.F.W. Pease, *IEEE Trans. Magn.* 33[1] (1997) 990-995.
2. E.S. Murdock, *IEEE Trans. Magn.* 28[5] (1992) 3078-3083.
3. D.N. Lambeth, E.M.T. Velu, G.H. Bellesis, L.L. Lee and D.E. Laughlin, *J. Appl. Phys.*, 79[8] (1996) 4496-4501.
4. M.H. Kryder, *MRS Bull.* 21[9] (1996) 17-19.
5. K. Ichihara, A. Kikitsu, K. Yusu, F. Nakamura and H. Ogiwara, *IEEE Trans. Magn.* 34[4] (1998) 1603-1605.
6. C. Chen, O. Kitakami and Y. Shimada, *IEEE Trans. Magn.* 35[5] (1999) 3466-3468.
7. S. Sung, C.B. Murray, D. Weller, L. Folks and A. Moser, *Science* 287 (2000) 1989-1991.
8. T.B. Massalski, H. Okamoto, P.R. Subramanian and L. Kacprzak (ed): *Binary Alloy Phase Diagrams*, 2nd ed. ASM International, Materials Park, Ohio, (1990) 1755.
9. A. Sakuma, *J. Phys. Soc. Jpn.* 63[8] (1994) 3053-3058.
10. T. Klemmer, D. Hoydick, H. Okumura, B. Zhang and W. A. Soffa, *Scripta Met. Mater.* 33[10/11] (1995) 1793-1805.
11. R.F.C. Farrow, D. Weller, R.F. Marks, M.F. Toney, A. Cebollada and G.R. Harp, *J. Appl. Phys.* 79[8] (1996) 5967-5969.
12. T. Shimatsu, J.C. Lodder, Y. Sugita and Y. Nakamura, *IEEE Trans. Magn.* 35[5] (1999) 2697-2699.
13. B. Bian, K. Sato, T. Ohkubo, Y. Hirotsu and A. Makino, *J. Magn. Soc. Jpn.* 23[1-2] (1999) 736-738.
14. C. Chen, O. Kitakami, S. Okamoto and Y. Shimada, *J. Appl. Phys.* 84[4] (1998) 2184-2188.
15. B.M. Lairson and B.M. Clemens, *Appl. Phys. Lett.* 63[10] (1993) 1438-1440.
16. M. Visokay and R. Sinclair, *Appl. Phys. Lett.* 66[13] (1995) 1692-1694.
17. S. Mitani, K. Takanashi, M. Sano, H. Fujimori, A. Osawa and H. Nakajima, *J. Magn. Magn. Mater.* 148[1-2] (1995) 163-164.
18. R.F.C. Farrow, D. Weller, R.F. Marks, M.F. Toney, S. Hom, G.R. Harp, A. Cebollada, *Appl. Phys. Lett.* 69[8] (1996) 1166-1168.
19. M. Watanabe and M. Homma, *Jpn. J. Appl. Phys.* 35[10A] (1996) L1264-L1267.
20. M.H. Hong, K. Horio and M. Watanabe, *J. Appl. Phys.* 84[8] (1998) 4403-4409.
21. B. Bian, K. Sato, Y. Hirotsu and A. Makino, *Appl. Phys. Lett.* 75[23] (1999) 3686-3688.
22. B. Bian, K. Sato, T. Ohkubo, Y. Hirotsu and A. Makino, *J. Electron Microsc.* 48[6] (1999) 753-760.
23. B. Bian, D.E. Laughlin, K. Sato and Y. Hirotsu, *J. Appl. Phys.* 87[9] (2000) 6962-6964.
24. B. Bian, D.E. Laughlin, K. Sato and Y. Hirotsu, *IEEE Trans. Magn.* (in press).
25. L. Néel, *Ann. Geophys.* 5 (1949) 99.
26. D.K. Lottice, R.M. White and E.D. Dahlberg, *Phys. Rev. Lett.* 67[3] (1991) 362-365.
27. Y. Park, S. Adenwalla, G.P. Felcher and S.D. Bader, *Phys. Rev. B* 52[17] (1995) 12779-12783.

# Topotactic Preparation of Preferentially Oriented BaTiO<sub>3</sub> and TiO<sub>2</sub> Thin Films on Polycrystalline Substrate

Qi Feng,\* Koji Kajiyoshi,<sup>†</sup> and Kazumichi Yamagisawa<sup>‡</sup>

Department of Advanced Materials Science, Faculty of Engineering, Kagawa University, 2217-20 Hayashi, Takamatsu 761-0396

<sup>†</sup>Research Laboratory of Hydrothermal Chemistry, Faculty of Science, Kochi University, Akebono, Kochi 780-8520

(Received September 19, 2002; CL-020807)

A layered titanate H<sub>1.08</sub>Ti<sub>1.73</sub>O<sub>4</sub> oriented thin film on stainless steel and Ti metal substrates was prepared by using an exfoliation-restacking technique. The layered titanate film can be topotactically transformed to anatase and rutile thin films with preferred orientation along [103] and [110] directions, respectively, by heat-treatment, and to a BaTiO<sub>3</sub> thin film with preferred orientation along [110] direction by hydrothermal treatment in a Ba(OH)<sub>2</sub> solution.

Preferentially oriented thin films of metal oxides are high performance materials for electronic devices. For the preparations of the preferentially oriented thin films, usually epitaxial crystal growth techniques are utilized.<sup>1-3</sup> In these cases, a single crystal substrate and lattice matching between the substrate crystal and the film crystal are necessary, meaning the high cost for the preparation of the epitaxial films. If a polycrystalline or amorphous substrate can be used for the oriented thin films, a low cost thin film process is possible. Some studies have indicated that the oriented thin films can be obtained on polycrystalline substrates or single crystal substrates without lattice matching by controlling growth direction of film crystal.<sup>4-6</sup> However, the control of crystal growth direction on a polycrystalline substrate is not easy in normal cases.

Recently, we have studied the preparation of BaTiO<sub>3</sub> and anatase from a titanate with a layered structure, and found that plate-like BaTiO<sub>3</sub> and anatase particles with preferred orientation can be obtained by hydrothermal treatment of the plate-like titanate particles in Ba(OH)<sub>2</sub> solution and distilled water, respectively.<sup>7</sup> The structural transformations from the layered titanate to BaTiO<sub>3</sub> and anatase are topotactic reactions. This result implies that if a oriented layered titanate film can be prepared on a polycrystalline or an amorphous substrate, the oriented BaTiO<sub>3</sub> and TiO<sub>2</sub> films would be obtained by using the topotactic structural transformation reactions.

For the preparations of layered metal oxide thin films with preferred orientation, recently, exfoliation and layer-by-layer assembly techniques have developed.<sup>8,9</sup> Titania nanostructured films have been obtained by heat-treatment of a layered titanate film prepared by using the layer-by-layer assembly technique.<sup>10</sup>

In the present study, we describe preparation of an oriented layered titanate thin film on stainless steel and Ti metal substrates by using an exfoliation-restacking technique, and preparation of oriented BaTiO<sub>3</sub> and TiO<sub>2</sub> thin films from the layered titanate film by using topotactic structural transformation reactions.

A layered H<sup>+</sup>-form titanate H<sub>1.07</sub>Ti<sub>1.73</sub>O<sub>4</sub>·nH<sub>2</sub>O (HTO) with a lepidocrocite-like layered structure was used as precursor, which was prepared from a layered titanate of K<sub>0.8</sub>Ti<sub>1.73</sub>Li<sub>0.27</sub>O<sub>4</sub>, as described previously.<sup>7</sup> HTO powder sample was exfoliated

into the nanosheets of elementary layer of its structure by reacting with a 0.1 M *n*-propylamine solution.<sup>11</sup> The titanium content in the resulted nanosheet colloidal solution was adjusted to 0.1 M. The HTO thin film was prepared by dipping the stainless steel substrate into the HTO nanosheet solution and then drying in air at room temperature. The HTO film with about 0.3 μm thickness was obtained by repeating the dipping and drying operation for 10 cycles. The HTO film has a layered structure with a basal spacing of 0.938 nm, which is larger than that of its precursor of HTO powder sample (0.922 nm) (Figure 1(b)). Only (0 k 0) diffraction peaks were observed, suggesting that the HTO nanosheets restack on the surface of the substrate and form a preferentially oriented film of the layered titanate after drying.

TiO<sub>2</sub> thin films can be obtained by heat-treatment of the HTO film in air. The HTO film retains the layered structure, but the intensity of the diffraction peaks decreased and the basal spacing changed to 0.933 nm after heat-treatment at 400 °C (Figure 1(c)). Anatase and rutile thin films were obtained after heat-treatment at 600 and 800 °C, respectively (Figure 1(d) and 1(e)). The anatase film shows much stronger (103) diffraction peak than that of the normal powder sample (anatase, JCPDS No. 21-1272), meaning (103) plane of anatase film parallels to the basal plane of the substrate. In the case of the rutile film, only (110) and (220) diffraction peaks were observed, indicating perfect preferred orientation along [110] direction. The preferred orientations

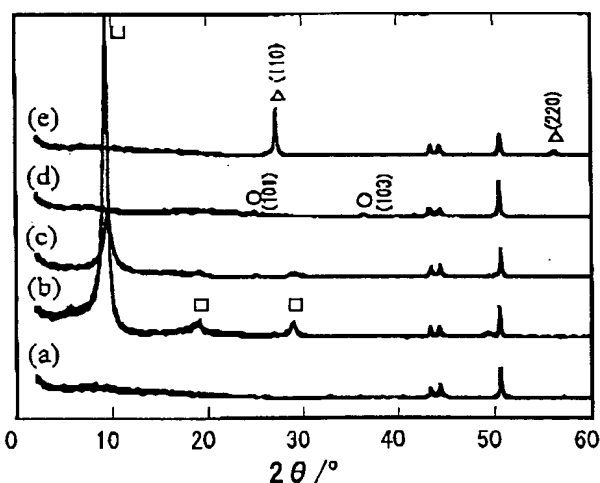


**Figure 1.** X-ray diffraction patterns of (a) stainless steel substrate, (b) HTO film, and the films obtained by heat-treatment of the HTO film at (c) 400, (d) 600, and (e) 800 °C for 2 h in air, respectively. Squares, circles, and triangles indicate layered titanate, anatase, rutile phases, respectively.

suggest that the formations of anatase and rutile from the layered titanate are dehydration topotactic structural transformation reactions.

A  $\text{BaTiO}_3$  film was prepared by hydrothermal treatment of the HTO film in a  $\text{Ba}(\text{OH})_2$  solution. Before the hydrothermal treatment, the HTO film was heated at  $400^\circ\text{C}$ . to prevent the dissolution of the HTO film by re-exfoliation reaction when the film was immersed in the solution. The  $\text{BaTiO}_3$  film with a cubic phase ( $\text{BaTiO}_3$ , JCPDS No. 31-174) can be obtained after the hydrothermal treatment in a 0.1 M  $\text{Ba}(\text{OH})_2$  solution at  $150^\circ\text{C}$  in a Teflon-lined, sealed stainless steel vessel (Figure 2(d)). The X-ray diffraction patterns showed very strong (110) diffraction peak and very weak peaks for other diffractions, indicating that  $\text{BaTiO}_3$  film with a preferred orientation along [110] direction was obtained. This result suggests that the formation of  $\text{BaTiO}_3$  phase is a topotactic structural transformation reaction, where  $\text{Ba}^{2+}$  migrate into the crystal bulk through the interlayer pathway and react with the  $\text{TiO}_6$  octahedral layers of HTO in the crystal bulk to form  $\text{BaTiO}_3$  in situ.<sup>7</sup>

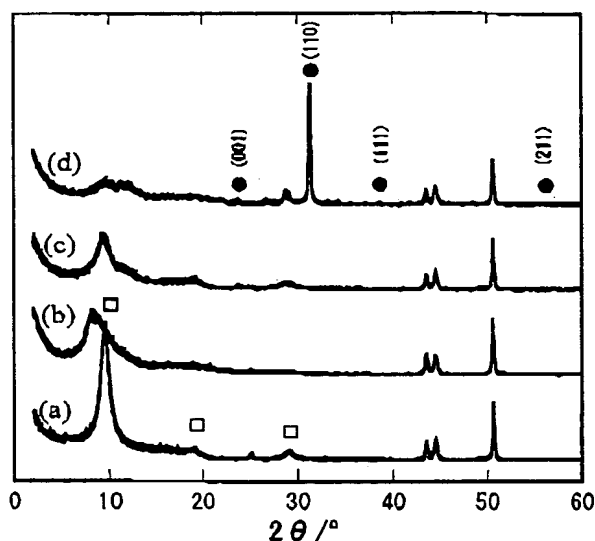


Figure 2. X-ray diffraction patterns of (a) the HTO film after heat-treatment at  $400^\circ\text{C}$ , and the films obtained by the hydrothermal treatment of the HTO film at  $150^\circ\text{C}$  for 20 h in (b) distilled water, (c) 0.01 M, and (d) 0.1 M  $\text{Ba}(\text{OH})_2$  solutions, respectively. Squares and circles indicate layered titanate and  $\text{BaTiO}_3$  phases, respectively.

The  $\text{BaTiO}_3$  film with preferred orientation along [110] direction can be prepared also on Ti metal substrate by using similar method, indicating the orientation direction is not

dependent on the properties of the substrate, but on the structure of HTO precursor. Preliminary capacitance and dielectric loss measurements were carried out on the  $\text{BaTiO}_3$  film with  $0.31\ \mu\text{m}$  thickness at an applied voltage of 0.1 V and  $25^\circ\text{C}$ . The dielectric constants and the dielectric losses are 570 and 11% at  $10^2\ \text{Hz}$ , and 440 and 18% at  $10^4\ \text{Hz}$  of frequency, respectively. It is notable that the dielectric constant is higher than that of  $\text{BaTiO}_3$  films prepared by other methods in same frequency range.<sup>12-15</sup>

In conclusion, the oriented  $\text{BaTiO}_3$  and  $\text{TiO}_2$  thin films could be prepared by using topotactic structural transformation reactions from the layered titanate precursor film. The preferred orientation direction of the films is dependent on the structure of the precursor, but not on the properties of the substrate.

This work was supported in part by Grants-in-Aid for Scientific Research (C) (No. 13650894) from Japan Society for the Promotion of Science.

#### References

1. K. Iijima, Y. Tomita, R. Takayama, and T. Ueda, *J. Appl. Phys.*, **60**, 361 (1986).
2. K. Kanno, S. Hayashi, R. Takayama, and T. Hirano, *Appl. Phys. Lett.*, **68**, 328 (1996).
3. H.-M. Christen, L. A. Boatner, J. D. Budai, M. F. Chishoim, L. A. Gea, R. J. Marrero, and D. P. Norton, *Appl. Phys. Lett.*, **68**, 1488 (1996).
4. C. H. Lee and S. J. Park, *J. Mater. Sci.: Mater. Electron.*, **1**, 219 (1990).
5. B. Yang, X. J. Zhang, S. T. Zhang, X. Y. Chen, Z. C. Wu, Y. F. Chen, Y. Y. Zhu, Z. G. Liu, and N. B. Ming, *Appl. Phys. Lett.*, **79**, 4559 (2001).
6. K. Kajiyoshi, N. Ishizawa, and M. Yoshimura, *J. Am. Ceram. Soc.*, **74**, 369 (1991).
7. Q. Feng, M. Hirasawa, and K. Yanagisawa, *Chem. Mater.*, **13**, 290 (2001).
8. R. E. Schaak and T. E. Mallouk, *Chem. Mater.*, **12**, 3427 (2000).
9. T. Sasaki, Y. Ebina, T. Tanaka, M. Harada, M. Watanabe, and G. Decher, *Chem. Mater.*, **13**, 4661 (2001).
10. T. Sasaki, Y. Ebina, K. Fukuda, T. Tanaka, M. Harada, and M. Watanabe, *Chem. Mater.*, **14**, 3524 (2002).
11. M. Iida, T. Sasaki, and M. Watanabe, *Chem. Mater.*, **10**, 3780 (1998).
12. K. Kajiyoshi, Y. Sakabe, and M. Yoshimura, *Jpn. J. Appl. Phys.*, **36**, 1209 (1997).
13. S. Venigalla, P. Bendale, and J. H. Adair, *J. Electrochem. Soc.*, **142**, 2101 (1993).
14. A. Tsuzuki, K. Kato, K. Kusumoto, and Y. Torii, *J. Mater. Sci.*, **33**, 3055 (1998).
15. B. S. Saha and S. B. Krupanidhi, *Appl. Phys. Lett.*, **79**, 111 (2001).

# Fabrication of $\langle 111 \rangle$ Oriented $\text{BaTiO}_3$ Bulk Ceramic by Reactive Templated Grain Growth Method

~~Tsutomu~~ SUGAWARA, Yoko NOMURA, Toshio KIMURA and Toshihiko TANI\*

~~School of Integrated Design Engineering, Graduate School of Science and Technology, Keio University,  
3-14-1, Hiyoshi, Kohoku-ku, Yokohama-shi 223-8522~~

~~\*Toyota Central Research and Development Laboratories, Inc., 41-1, Yokomichi, Nagakute, Aichi-gun, Aichi 480-1192~~

## 反応性テンプレート粒成長法による $\langle 111 \rangle$ 配向性 $\text{BaTiO}_3$ バルクセラミックスの製造

菅原 努・野村陽子・木村敏夫・谷 俊彦\*

慶應義塾大学大学院理工学研究科, 223-8522 横浜市港北区日吉 3-14-1

\*(株)豊田中央研究所, 480-1192 愛知県愛知郡長久手町横道 41-1

A polycrystalline  $\text{BaTiO}_3$  bulk ceramic with a preferred  $\langle 111 \rangle$  orientation was fabricated by the reactive templated grain growth method. A green compact was made by tape-casting of slurry containing plate-like  $\text{Ba}_6\text{Ti}_{17}\text{O}_{40}$  template particles and  $\text{BaCO}_3$  powder. Single phase  $\text{BaTiO}_3$  was obtained by calcining the green compact at  $1000^\circ\text{C}$ . The calcined compacts were sintered between  $1250$  and  $1400^\circ\text{C}$ . The degree of orientation increased with an increase in the sintering temperature. Growth of  $\langle 111 \rangle$ -oriented  $\text{BaTiO}_3$  grains originated from the  $\text{Ba}_6\text{Ti}_{17}\text{O}_{40}$  particles is responsible for the increase in the degree of orientation.

[Received June 29, 2001; Accepted August 9, 2001]

~~Key-words: Barium titanate, Grain orientation, Reactive templated grain growth~~

### 1. Introduction

Grain orientation is an important technique to improve performance of ferroelectric ceramics.<sup>1)-5)</sup> There have been two fabrication methods to prepare grain-oriented ferroelectric ceramics; one aligns grains by applying pressure during sintering<sup>1),2),6)</sup> and another prepares green compacts with aligned particles.<sup>9)-11)</sup> In the latter method, plate- or needle-like powder particles are aligned in a green compact by tape-casting, extrusion, and slip-casting. In these methods, grain growth during sintering<sup>6)</sup> and particle growth during Ostwald ripening in molten salt<sup>12)</sup> are necessary to be anisotropic. Therefore, these methods are only applicable to materials with low symmetry, such as those belonging to the bismuth layer-structured ferroelectrics and tungsten-bronze-type niobates.

Many compounds with good dielectric and piezoelectric properties have a crystal structure with high symmetry, such as regular perovskite. To obtain grain-oriented ceramics for these compounds, the reactive templated grain growth (abbreviated as RTGG) method<sup>3)</sup> has been employed, in which ceramics are made by *in situ* reaction and successive sintering using starting material powders with a plate- or needle-shape. Thus, grain-oriented  $\text{Bi}_{0.5}(\text{Na}_{0.45}\text{K}_{0.15})_{0.5}\text{TiO}_3$  with the perovskite structure was fabricated, and significant improvement of the piezoelectric properties due to grain orientation was reported.<sup>3)</sup> Because this method requires a starting material with an anisotropic shape and the topotactic or epitaxial relation between the starting material and product,<sup>13)</sup> the application of this method has been restricted to a few compounds, and the selection of starting material is important to apply this method to other compounds.

The primary purpose of this note is to investigate the feasibility of fabricating  $\text{BaTiO}_3$  with a significant  $\langle 111 \rangle$  orientation. The  $\langle 111 \rangle$ -oriented  $\text{BaTiO}_3$  ceramics would exhibit a hysteresis-free strain vs. electric field curve as shown in a single crystal.<sup>14)</sup>  $\text{Ba}_6\text{Ti}_{17}\text{O}_{40}$  (abbreviated as B6T17) was selected for the starting material from two points of view. The powder with an anisotropic shape is expected to be obtained from the crystal structure,<sup>15)</sup> and the  $\langle 111 \rangle$

grain-orientation is expected from the topotactic relation between crystal axes of B6T17 and  $\text{BaTiO}_3$ , i.e.,  $(001)_{\text{B6T17}} // (111)_{\text{BaTiO}_3}$ , and  $[010]_{\text{B6T17}} // [110]_{\text{BaTiO}_3}$ .<sup>16),17)</sup> The crystal structure of B6T17 is monoclinic with  $a = 0.9887$  nm,  $b = 1.7096$  nm,  $c = 1.8918$  nm, and  $\beta = 98.72^\circ$ .<sup>18)</sup>

### 2. Experimental

Plate-like B6T17 was prepared from  $\text{BaTiO}_3$  and  $\text{TiO}_2$  in the presence of NaCl.  $\text{BaTiO}_3$  and  $\text{TiO}_2$ , with the average particle sizes of  $0.5$  and  $0.6 \mu\text{m}$  respectively, were mixed in a  $6:11$  molar ratio with a ball mill for  $24$  h using ethanol as a medium. The dried mixture was mixed with an equal weight of NaCl in an electrically-driven agate mortar and pestle for  $30$  min, and then heated at  $1150^\circ\text{C}$  for  $1$  h. NaCl was removed from the reaction product by washing with distilled water more than  $10$  times.

Two preparation methods of slurry for tape-casting were employed. In the first method, B6T17 and  $\text{BaCO}_3$  in a  $1:11$  molar ratio were mixed with a solvent ( $60$  vol% toluene- $40$  vol% ethanol) in a centrifugal ball mill for  $3$  h, and then poly(vinyl butyral) (binder) and di-*n*-butyl phthalate (plasticizer) were added and mixed for  $2$  h. In the second method, B6T17 was mixed with the solvent containing a small amount of poly(vinyl butyral) in the centrifugal ball mill for  $2$  h. Then,  $\text{BaCO}_3$  was added and mixed for  $1.5$  h. Finally, remaining poly(vinyl butyral) and di-*n*-butyl phthalate were added and mixed for  $2$  h.

The slurries were tape-cast onto a plastic film. Green sheets were cut, stacked, and pressed at  $80^\circ\text{C}$  and  $110$  MPa for  $3$  min. The thickness of the compacts was about  $2$  mm. The compacts were further cut into small pieces ( $10$  mm  $\times$   $10$  mm).

The binder and plasticizer were burned out at  $600^\circ\text{C}$  for  $2$  h (heating rate was  $50^\circ\text{C}/\text{h}$ ). Then, the compacts were calcined at  $1000^\circ\text{C}$  for  $2$  h (heating rate was  $100^\circ\text{C}/\text{h}$ ). The formation of  $\text{BaTiO}_3$  was completed at this stage, as judged by X-ray diffraction analysis. The calcined compacts were cooled to room temperature and pressed isostatically (CIP) at  $100$  MPa to increase green density, because the reaction between B6T17 and  $\text{BaCO}_3$  caused expansion of the com-

pacts. The CIP-ed compacts were sintered between 1250 and 1400°C for 2 h (the heating rate was 100°C/h).

The phases present and the degree of orientation were determined by X-ray diffraction (XRD) analysis using Cu K $\alpha$  radiation on the major surface of compacts (parallel to the casting direction). The sintered compacts were polished before XRD measurement to examine the grain orientation in the bulk. The degree of orientation,  $F$ , was calculated by the following equations (Lotgering method<sup>[18]</sup>),

$$F = \frac{P - P_0}{1 - P_0} \quad (1)$$

$$P = \frac{I_{(111)}}{\sum I_{(hkl)}} \quad \text{and} \quad P_0 = \frac{I_0(111)}{\sum I_0(hkl)} \quad (2)$$

where  $I$  and  $I_0$  are the peak heights for the sintered compact and randomly oriented BaTiO<sub>3</sub>, respectively, and {111} and {hkl} stand for the Miller indices. The diffraction lines between  $2\theta = 20$  and  $60^\circ$  were used to calculate  $\sum I_{(hkl)}$  and  $\sum I_0(hkl)$ . The microstructure was observed on fracture surfaces perpendicular to the major surface of sintered compacts with a scanning electron microscope (SEM). The density of sintered compacts was determined by the Archimedes method.

### 3. Results and discussion

Figure 1 shows the SEM photograph of the B6T17 powder. The powder was mainly composed of plate-like particles with the length of plate face between 10 and 20  $\mu\text{m}$  and a thickness of about 3  $\mu\text{m}$ . Figure 2 shows the XRD pattern



Fig. 1. SEM photograph of B6T17 powder.

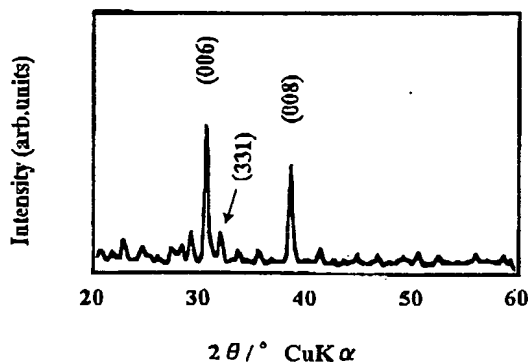


Fig. 2. XRD pattern of B6T17 powder. The sample was prepared by tape-casting.

of the B6T17 powder. To examine the crystallographic direction, the sample for XRD measurement was prepared by tape-casting. All XRD peaks were assigned to those of B6T17 (JCPDS No. 35-817). While the most intense peak of B6T17 with random orientation is (331) at  $2\theta = 31.3^\circ$ , the XRD pattern in Fig. 2 had the intense (006) and (008) peaks at  $2\theta = 28.6^\circ$  and  $38.5^\circ$ , respectively, indicating that the <001> direction of B6T17 lies perpendicular to the plate face, because the plate face of the particles aligned parallel to the major face of the sheet.

Figure 3 shows the XRD pattern of the RTGG-processed compact sintered at 1400°C for 2 h as well as BaTiO<sub>3</sub> powder. The RTGG-processed compact was made from the slurry prepared by the first preparation method. The most intense peak was {111} of BaTiO<sub>3</sub> for the RTGG-processed compact, while it was {110} for the BaTiO<sub>3</sub> powder. The degree of orientation of the RTGG-processed compact was 0.25, which was smaller than expected.

Figure 4 shows an example of microstructure on a fracture surface perpendicular to the major face of the compact after binder burn-out. The plate-like B6T17 particles were

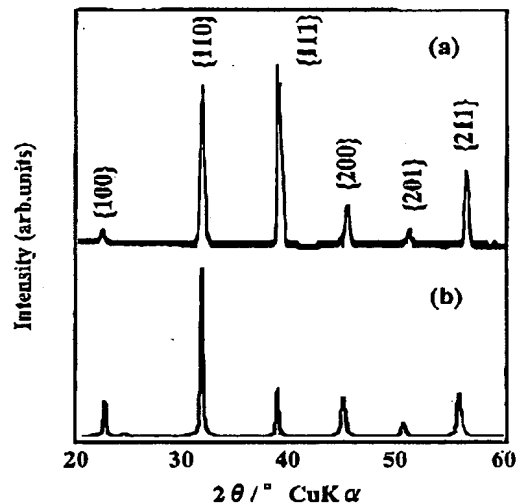


Fig. 3. XRD patterns of (a) RTGG-processed sample and (b) BaTiO<sub>3</sub> powder. The RTGG-processed sample was made from the slurry prepared by the first preparation method, and was sintered at 1400°C for 2 h.

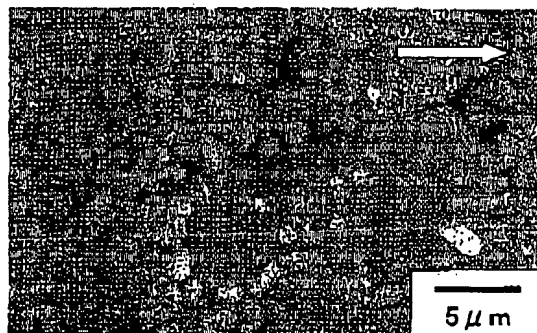


Fig. 4. Microstructure of fracture surface perpendicular to the major face of cast compact after binder burn-out at 600°C for 2 h. The compact was made from the slurry prepared by the first preparation method. The casting direction is indicated by the arrow.

hardly observed, and if observed, the orientation was rather random. The large particle in Fig. 4 was B6T17 and plate face was observed. The side face of a plate-like particle should be observed in the fracture surface perpendicular to the major face of the compact, if the B6T17 particles were aligned by tape-casting.

The observation of the microstructure of green compact indicates that the small degree of orientation shown in Fig. 3 is caused by the mis-alignment of B6T17 particles in the cast sheet. Probably, agglomerates of B6T17 and  $\text{BaCO}_3$  were formed in the slurry and disturbed the alignment of B6T17 particles. The fact that B6T17 particles were hardly observed on the fracture surface perpendicular to the casting direction indicates that B6T17 particles are covered with  $\text{BaCO}_3$  particles to form agglomerates with an isotropic shape.

To improve the dispersion of powder particles in the slurry, the second method of slurry preparation was employed, since a small amount of poly(vinyl butyral) acts as a dispersant.<sup>19)</sup> Figure 5 shows the microstructure of a fracture surface perpendicular to the major face of the compact made from the slurry prepared by the second method. To show the particle alignment clearly, the compact after binder burn-out was fractured and immersed in a  $\text{HNO}_3$  solution to remove a part of  $\text{BaCO}_3$ . Figure 5 indicates that tape-casting of the slurry resulted in the alignment of B6T17 particles with their plate face parallel to the casting direction.

Figure 6 shows the XRD patterns of the compacts sintered at various temperatures for 2 h, measured at the major face parallel to the casting direction. The most intense peak of the sintered compacts was (111), indicating that <111> of many grains lies perpendicular to the casting direction. This preferred orientation is expected from the orientation relation between B6T17 and  $\text{BaTiO}_3$ .<sup>15),16)</sup> The result shown in Fig. 6 indicates that the topotactic relation between B6T17 and  $\text{BaTiO}_3$  is retained during the formation of  $\text{BaTiO}_3$ .

The degree of orientation was dependent on the sintering temperature as shown in Fig. 6; an increase in the sintering temperature increased the degree of orientation.

Figure 7 shows the microstructures of fracture surfaces perpendicular to the major face of the compacts. The sample sintered at 1250°C was composed of plate-like and equiaxed grains. The formation of plate-like grains gives the preferred <111> orientation, whereas the orientation of equiaxed grains is random, as judged from Fig. 6(a). The diffusion of Ba into plate-like B6T17 resulted in the formation of plate-like  $\text{BaTiO}_3$  grains.<sup>20)</sup> The origin of equiaxed grains is not certain. One possible origin is the presence of equiaxed particles in the B6T17 powder (Fig. 1). Another possible origin is the fragmentation of plate-like  $\text{BaTiO}_3$  grain into small grains during the  $\text{BaTiO}_3$  formation, because the plate-like  $\text{BaTiO}_3$  grain is polycrystal. Plate-like character was maintained up to 1300°C, while grain growth was evident at and above 1300°C. At 1350 and 1400°C, plate-like character was lost and grains had an irregular shape, although the <111> direction of most grains lay perpendicular to the major face of the compact (Fig. 6). Growth of <111>-oriented grains at the expense of mis-oriented grains is responsible for the increase in the degree of orientation.<sup>21)</sup>

Large pores existed in the sample sintered at 1250°C, and these pores accumulated between the grains with plate-like character at 1300°C. These pores were hardly eliminated by sintering at higher temperatures, as shown in Fig. 7. The density of the samples sintered at 1250, 1300, 1350 and 1400°C was 43, 62, 81 and 81% of theoretical, respectively. The measurement of electrical properties, especially piezoelectric property, was difficult because of the low density. The attempts to increase the sintered density are under way.



Fig. 5. Microstructure of fracture surface perpendicular to the major face of cast compact after binder burn-out at 600°C for 2 h. The compact was made from the slurry prepared by the second preparation method. The compact was treated in a  $\text{HNO}_3$  solution to remove a part of  $\text{BaCO}_3$  and clearly observe the alignment of B6T17 particles. The casting direction is indicated by the arrow.

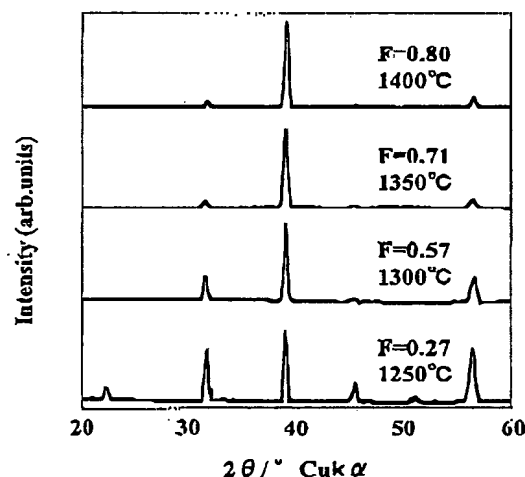


Fig. 6. XRD patterns of compacts sintered at various temperatures for 2 h. The compacts were made from the slurry prepared by the second preparation method. The  $F$  values indicate the degree of orientation.

#### 4. Conclusions

A polycrystalline  $\text{BaTiO}_3$  bulk ceramic with a preferred <111> orientation was fabricated by the reactive templated grain growth method, using plate-like B6T17 particles with the <001> direction perpendicular to the plate face. Alignment of B6T17 particles was achieved by tape-casting of a slurry containing B6T17 and  $\text{BaCO}_3$  powders. The dispersion of powder particles in the slurry was important to align the plate-like B6T17 particles. Plate-like  $\text{BaTiO}_3$  grains with the <111> direction perpendicular to the casting direction were formed during the reaction between B6T17 and  $\text{BaCO}_3$ . Thus, the compact was composed of plate-like  $\text{BaTiO}_3$  grains and equiaxed  $\text{BaTiO}_3$  grains with random orientation. Growth of <111>-oriented grains at the expense of randomly-oriented grains increased the degree of orientation.

#### References

- 1) Igarashi, H., Matsunaga, K., Tanai, T. and Okazaki, K., *Am. Ceram. Soc. Bull.*, 57, 815-17 (1978).

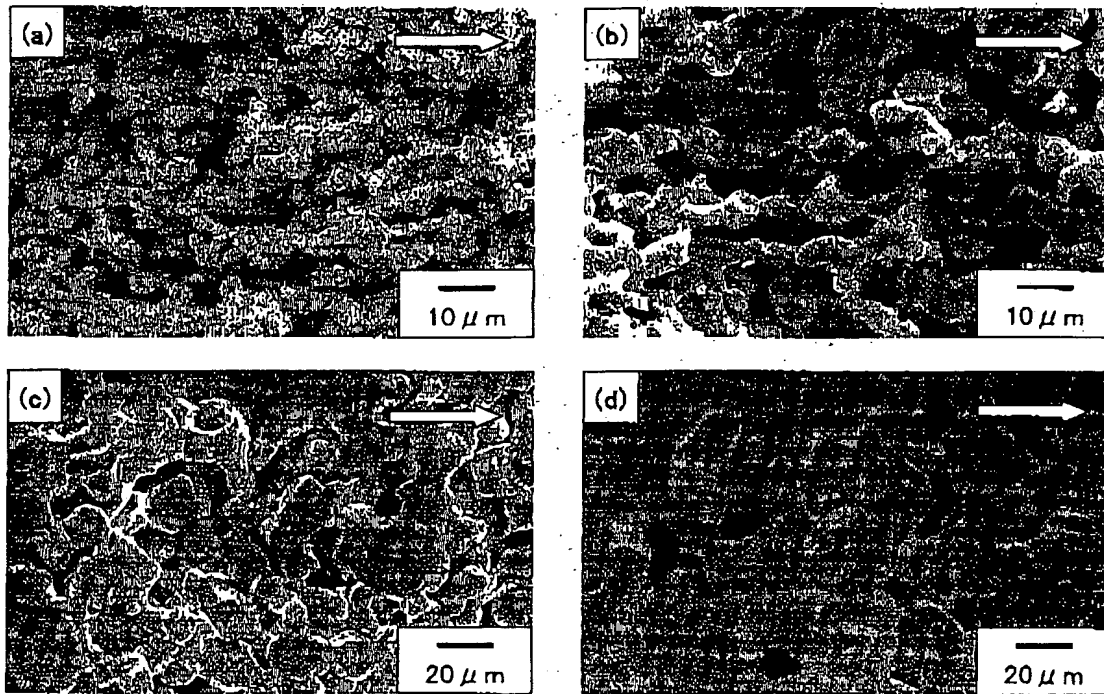


Fig. 7. Microstructures of fracture surfaces perpendicular to the major face of compacts sintered at (a) 1250°, (b) 1300°, (c) 1350°C and (d) 1400°C for 2 h. The compacts were made from the slurry prepared by the second preparation method. The casting direction is indicated by the arrows.

- 2) Takenaka, T. and Sakata, K., *Jpn. J. Appl. Phys.*, 19, 31-39 (1980).
- 3) Tani, T., *J. Korean Phys. Soc.*, 32, S1217-20 (1998).
- 4) Hong, S.-H., Trolier-McKinstry, S. and Messing, G. L., *J. Am. Ceram. Soc.*, 83, 113-18 (2000).
- 5) Duran, C., Trolier-McKinstry, S. and Messing, G. L., *J. Am. Ceram. Soc.*, 83, 2203-13 (2000).
- 6) Kimura, T., Yoshimoto, T., Iida, N., Fujita, Y. and Yamaguchi, T., *J. Am. Ceram. Soc.*, 72, 85-89 (1989).
- 7) Lin, S.-H., Swartz, S. L., Shulze, W. A. and Biggers, J. V., *J. Am. Ceram. Soc.*, 66, 881-84 (1983).
- 8) Watanabe, H., Kimura, T. and Yamaguchi, T., *J. Am. Ceram. Soc.*, 74, 139-47 (1991).
- 9) Brahmaroutu, B., Messing, G. L., Trolier-McKinstry, S. and Selvaraj, U., Proceedings of the Tenth International Symposium on Applications of Ferroelectrics, East Brunswick, NJ, August 18-21, Ed. by Kulwicki, B. M., Amin, A. and Safari, A. (1996) pp. 883-88.
- 10) Horn, J. A., Zhang, S. C., Selvaraj, U., Messing, G. L. and Trolier-McKinstry, S., *J. Am. Ceram. Soc.*, 82, 921-26 (1999).
- 11) Takeuchi, T., Tani, T. and Saito, Y., *Jpn. J. Appl. Phys. Part 1*, 38, 5553-56 (1999).
- 12) Kimura, T. and Yamaguchi, T., *Ceram. Int.*, 9, 13-17 (1983).
- 13) Sano, Y. and Tani, T., *Ferroelectrics*, 224, 793-800 (1999).
- 14) Wada, S., Suzuki, S., Noma, T., Suzuki, T., Osada, M., Kaki-hana, M., Park, S.-E., Cross, L. E. and Shrout, T. R., *Jpn. J. Appl. Phys. Part 1*, 38, 5505-11 (1999).
- 15) Hofmeister, W., Tillmanns, E. and Baur, W. H., *Acta Cryst., Sect. C*, 40, 1510-12 (1984).
- 16) Krasevec, V., Drofenik, M. and Kolar, D., *J. Am. Ceram. Soc.*, 70, C193-95 (1987).
- 17) Senz, S., Graff, A., Blum, W., Hesse, D. and Abicht, H.-P., *J. Am. Ceram. Soc.*, 81, 1317-21 (1998).
- 18) Lotgering, F. K., *J. Inorg. Nucl. Chem.*, 9, 113-23 (1959).
- 19) Watanabe, H., Kimura, T. and Yamaguchi, T., *J. Am. Ceram. Soc.*, 72, 289-93 (1989).
- 20) Suyama, Y. and Kato, A., *Bull. Chem. Soc. Jpn.*, 50, 1361-66 (1977).
- 21) Seabaugh, M. M., Messing, G. L. and Vaudin, M. D., *J. Am. Ceram. Soc.*, 83, 3109-16 (2000).

**This Page is Inserted by IFW Indexing and Scanning  
Operations and is not part of the Official Record**

**BEST AVAILABLE IMAGES**

Defective images within this document are accurate representations of the original documents submitted by the applicant.

Defects in the images include but are not limited to the items checked:

- ☐ **BLACK BORDERS**
- ☐ **IMAGE CUT OFF AT TOP, BOTTOM OR SIDES**
- ☐ **FADED TEXT OR DRAWING**
- ☐ **BLURRED OR ILLEGIBLE TEXT OR DRAWING**
- ☐ **SKEWED/SLANTED IMAGES**
- ☐ **COLOR OR BLACK AND WHITE PHOTOGRAPHS**
- ☐ **GRAY SCALE DOCUMENTS**
- ☐ **LINES OR MARKS ON ORIGINAL DOCUMENT**
- ☐ **REFERENCE(S) OR EXHIBIT(S) SUBMITTED ARE POOR QUALITY**
- ☐ **OTHER:** \_\_\_\_\_

**IMAGES ARE BEST AVAILABLE COPY.**

**As rescanning these documents will not correct the image problems checked, please do not report these problems to the IFW Image Problem Mailbox.**

**This Page is Inserted by IFW Indexing and Scanning  
Operations and is not part of the Official Record**

**BEST AVAILABLE IMAGES**

Defective images within this document are accurate representations of the original documents submitted by the applicant.

Defects in the images include but are not limited to the items checked:

- ☐ **BLACK BORDERS**
- ☐ **IMAGE CUT OFF AT TOP, BOTTOM OR SIDES**
- ☐ **FADED TEXT OR DRAWING**
- ☐ **BLURRED OR ILLEGIBLE TEXT OR DRAWING**
- ☐ **SKEWED/SLANTED IMAGES**
- ☐ **COLOR OR BLACK AND WHITE PHOTOGRAPHS**
- ☐ **GRAY SCALE DOCUMENTS**
- ☐ **LINES OR MARKS ON ORIGINAL DOCUMENT**
- ☐ **REFERENCE(S) OR EXHIBIT(S) SUBMITTED ARE POOR QUALITY**
- ☐ **OTHER:** \_\_\_\_\_

**IMAGES ARE BEST AVAILABLE COPY.**

**As rescanning these documents will not correct the image problems checked, please do not report these problems to the IFW Image Problem Mailbox.**